



universität
wien

MASTERARBEIT / MASTER'S THESIS

Titel der Masterarbeit / Title of the Master's Thesis

„Ionothermal versus hydrothermal synthesis at the
example of the CdO–MO–As₂O₅–(H₂O/IL)-system“

verfasst von / submitted by

Sabrina Stefanie Gerger, BSc.

angestrebter akademischer Grad / in partial fulfilment of the requirements for the degree of
Master of Science (MSc.)

Wien, 2016 / Vienna 2016

Studienkennzahl lt. Studienblatt /
degree programme code as it appears on
the student record sheet:

A 066 815

Studienrichtung lt. Studienblatt /
degree programme as it appears on
the student record sheet:

Erdwissenschaften

Betreut von / Supervisor:

Univ.-Prof. Dr. Ronald Miletich-Pawliczek

Mitbetreut von / Co-Supervisor:

Dr. Tamara Đorđević

ABSTRACT

Within the scope of systematic research on mineral-related arsenates in the system $\text{CdO}-\text{MO}-\text{As}_2\text{O}_5-(\text{H}_2\text{O}/\text{IL})$ the two polymorphs of $(\text{C}_6\text{H}_{11}\text{N}_2)_2[\text{CdBr}_4]$, α - $(\text{C}_6\text{H}_{11}\text{N}_2)_2[\text{CdBr}_4]$ (**1**) and β - $(\text{C}_6\text{H}_{11}\text{N}_2)_2[\text{CdBr}_4]$ (**2**) and a Zn-containing arsenate, $\text{Zn}_9(\text{AsO}_4)_6(\text{H}_2\text{O})_4$ (**3**), were synthesised under ionothermal conditions using the ionic liquid (IL) 1-ethyl-3-methylimidazolium bromide, $\text{C}_6\text{H}_{11}\text{N}_2\text{Br}$. Furthermore, a new Ni-bearing mineral-like Cd-arsenate, $\text{Cd}_{4.65}\text{Ni}_{0.35}(\text{H}_2\text{O})_4(\text{AsO}_4)_2(\text{HAsO}_4)_2$ (**4**), has been synthesised under hydrothermal conditions. The different approaches in the synthesis of mineral-related arsenates, the temperature treatment and the role of the different solvents were also discussed.

All compounds were characterised using single-crystal X-ray diffraction, SEM/EDS analysis and vibrational spectroscopy: **1** monoclinic, $P2_1/c$, $a = 13.975(3) \text{ \AA}$, $b = 10.343(2) \text{ \AA}$, $c = 14.895(3) \text{ \AA}$, $\beta = 94.35(3)^\circ$, $V = 2146.8(8) \text{ \AA}^3$, $Z = 4$, $R_1 = 0.039$; **2** tetragonal, $I4_1/a$, $a = 14.863(2) \text{ \AA}$, $c = 20.600(2) \text{ \AA}$, $V = 4550.9(16) \text{ \AA}^3$, $Z = 22$, $R_1 = 0.042$; **3** triclinic, $P\bar{1}$, $a = 6.6983(13) \text{ \AA}$, $b = 9.1885(18) \text{ \AA}$, $c = 10.146(2) \text{ \AA}$, $\alpha = 69.44(3)^\circ$, $\beta = 94.35(3)^\circ$, $\gamma = 75.78(3)^\circ$, $V = 560.6(2) \text{ \AA}^3$, $Z = 1$, $R_1 = 0.0287$; **4** monoclinic $C2/c$, $a = 18.375(4) \text{ \AA}$, $b = 9.5395(19) \text{ \AA}$, $c = 9.977(2) \text{ \AA}$, $\beta = 96.19(3)^\circ$, $V = 1738.6(6) \text{ \AA}^3$, $Z = 4$, $R_1 = 0.0296$. $\text{Zn}_9(\text{AsO}_4)_6(\text{H}_2\text{O})_4$ (**3**) is a known compound but for the first time synthesised under ionothermal conditions using the ionic liquid [emim]Br as solvent and the positions of the hydrogen atoms have been determined and refined. $\text{Cd}_{4.65}\text{Ni}_{0.35}(\text{H}_2\text{O})_4(\text{AsO}_4)_2(\text{HAsO}_4)_2$ (**4**) is a new nickel-bearing cadmium-arsenate with a mineral-like structure.

KURZZUSAMMENFASSUNG

Im Rahmen von systematischen Untersuchungen von mineralähnlichen Arsenaten in dem System $\text{CdO}-\text{MO}-\text{As}_2\text{O}_5-(\text{H}_2\text{O}/\text{IL})$ wurden zwei Polymorphe von $(\text{C}_6\text{H}_{11}\text{N}_2)_2[\text{CdBr}_4]$, α - $(\text{C}_6\text{H}_{11}\text{N}_2)_2[\text{CdBr}_4]$ (**1**) und β - $(\text{C}_6\text{H}_{11}\text{N}_2)_2[\text{CdBr}_4]$ (**2**) und ein Zink-Arsenat, $\text{Zn}_9(\text{AsO}_4)_6(\text{H}_2\text{O})_4$ (**3**), unter ionothermalen Bedingungen mit der ionischen Flüssigkeit (IF) 1-Ethyl-3-Methylimidazolium Bromid, $\text{C}_6\text{H}_{11}\text{BrN}_2$, synthetisiert. Weiters wurde ein Ni-haltiges, mineralähnliches Cd-Arsenat, $\text{Cd}_{4.65}\text{Ni}_{0.35}(\text{H}_2\text{O})_4(\text{AsO}_4)_2(\text{HAsO}_4)_2$ (**4**), unter hydrothermalen Bedingungen synthetisiert. Die unterschiedlichen Ansätze der Synthese von mineralähnlichen Arsenaten, die Temperaturbehandlung und die Rolle der unterschiedlichen Lösungsmittel wurden auch behandelt.

Alle Verbindungen wurden mithilfe von Einkristalldiffraktometrie, SEM/EDS und Schwingungsspektroskopie charakterisiert: **1** monoklin, $P2_1/c$, $a = 13,975(3) \text{ \AA}$, $b = 10,343(2) \text{ \AA}$, $c = 14,895(3) \text{ \AA}$, $\beta = 94,35(3)^\circ$, $V = 2146,8(8) \text{ \AA}^3$, $Z = 4$, $R_1 = 0,039$; **2** tetragonal, $I4_1/a$, $a = 14,863(2) \text{ \AA}$, $c = 20,600(2) \text{ \AA}$, $V = 4550,9(16) \text{ \AA}^3$, $Z = 22$, $R_1 = 0,042$; **3** triklin, $P\bar{1}$, $a = 6,6983(13) \text{ \AA}$, $b = 9,1885(18) \text{ \AA}$, $c = 10,146(2) \text{ \AA}$, $\alpha = 69,44(3)^\circ$, $\beta = 94,35(3)^\circ$, $\gamma = 75,78(3)^\circ$, $V = 560,6(2) \text{ \AA}^3$, $Z = 1$, $R_1 = 0,0287$; **4** monoclinic $C2/c$, $a = 18,375(4) \text{ \AA}$, $b = 9,5395(19) \text{ \AA}$, $c = 9,977(2) \text{ \AA}$, $\beta = 96,19(3)^\circ$, $V = 1738,6(6) \text{ \AA}^3$, $Z = 4$, $R_1 = 0,0296$. $\text{Zn}_9(\text{AsO}_4)_6(\text{H}_2\text{O})_4$ (**3**) ist eine bekannte Verbindung, wurde aber das erste Mal unter ionothermalen Bedingungen synthetisiert und die Positionen der Wasserstoffatome wurde bestimmt und verfeinert. $\text{Cd}_{4.65}\text{Ni}_{0.35}(\text{H}_2\text{O})_4(\text{AsO}_4)_2(\text{HAsO}_4)_2$ (**4**) ist ein neues Ni-haltiges Cd-Arsenat mit einer mineralähnlichen Struktur.

TABLE OF CONTENTS

ABSTRACT.....	III
KURZZUSAMMENFASSUNG	V
TABLE OF CONTENTS	VII
LIST OF FIGURES	IX
LIST OF TABLES.....	XI
1 INTRODUCTION	15
1.1 Arsenic.....	15
1.2 Cadmium	16
1.3 Cadmium arsenates.....	16
2 METHODOLOGY	19
2.1 Hydrothermal synthesis	19
2.2 Ionothermal synthesis.....	20
2.2.1 Ionic liquids	20
2.2.1.1 1-Ethyl-3-methyl-imidazolium bromide: [emim]Br	22
2.3 Single crystal X-ray diffraction.....	23
2.4 Raman Spectroscopy	25
2.5 Infrared Spectroscopy	27
2.6 Scattered electron microscopy	29
3 EXPERIMENTAL.....	31
3.1 Synthesis of the single crystals.....	31
3.2 Single crystal X-ray diffraction measurements	34
3.3 Raman spectroscopy	37
3.4 Infrared spectroscopy	37
3.5 Scanning electron microscopy/energy dispersive spectroscopy	38
4 RESULTS	39
4.1 Results of the synthesis.....	39
4.2 α - and β -(C ₆ H ₁₁ N ₂) ₂ [CdBr ₄]	41
4.2.1 α -(C ₆ H ₁₁ N ₂) ₂ [CdBr ₄].....	43
4.2.2 β -(C ₆ H ₁₁ N ₂) ₂ [CdBr ₄]	48
4.2.3 Infrared spectra of α - and β -(C ₆ H ₁₁ N ₂) ₂ [CdBr ₄].....	52
4.3 Zn ₉ (AsO ₄) ₆ (H ₂ O) ₄	54
4.3.1 Structure description	55
4.3.2 Raman Spectra of Zn ₉ (AsO ₄) ₆ (H ₂ O) ₄	64
4.4 Cd _{4.65} Ni _{0.35} (H ₂ O) ₄ (AsO ₄) ₂ (HAsO ₄) ₂	65
4.4.1 Structure description	66

4.4.2	Raman spectra of $\text{Cd}_{4.65}\text{Ni}_{0.35}(\text{H}_2\text{O})_4(\text{AsO}_4)_2(\text{HAsO}_4)_2$	73
5	CONCLUSION	75
6	REFERENCES	77
7	ACKNOWLEDGMENT	83
8	INDEPENDENCE DECLARATION	85

LIST OF FIGURES

Figure 1.	A graphical representation of the distribution of arsenic in minerals according to the data of Strunz and Nickel (2001).	15
Figure 2.	Morey-autclave with Teflon vessel.	21
Figure 3.	Common cations and anions for ionic liquids (Moosavi, 2013).	21
Figure 4.	The skeletal formula of 1-Ethyl-3-methylimidazoliumbromide.....	22
Figure 5.	Simplified energy level diagrams which describe the difference between Infrared absorption (1), Rayleigh scattering (2) and Raman scattering (3) (Nasdala et al., 2004).....	26
Figure 6.	A schematic diagram of an electron column (Goldstein et al., 2003).....	30
Figure 7.	Temperature gradient for the four synthesis cycles.	32
Figure 8.	A schematic illustration of the synthesis of tetrahedral-octahedral frameworks under hydrothermal (left) and ionothermal (right) conditions.	40
Figure 9.	The sample-material with α -(a) and β -($C_6H_{11}N_2$) ₂ [CdBr ₄] (b) and images of α - (c, e) and β -($C_6H_{11}N_2$) ₂ [CdBr ₄] (d, f). (c) and (d) are light microscope images and (e) and (f) are BSE images.	42
Figure 10.	An overview of the structure of α -($C_6H_{11}N_2$) ₂ [CdBr ₄] (a), the hydrogen bonds (b) and the [emim] cation in detail with different perspectives of α - ($C_6H_{11}N_2$) ₂ [CdBr ₄] (c).....	44
Figure 11.	An overview of the structure of β -($C_6H_{11}N_2$) ₂ [CdBr ₄] (a), the hydrogen bonds (b, c) and the [emim] cation of β -($C_6H_{11}N_2$) ₂ [CdBr ₄] (d).	49
Figure 12.	IR-spectra of α -($C_6H_{11}N_2$) ₂ [CdBr ₄] (blue) and β -($C_6H_{11}N_2$) ₂ [CdBr ₄] (red).	53

- Figure 13.** The sample material with $Zn_9(AsO_4)_6(H_2O)_4$ (a) and the single crystal (b, c). (b) is a light microscope image and (c) is a BSE image of $Zn_9(AsO_4)_6(H_2O)_4$ 54
- Figure 14.** An illustration of the whole structure of $Zn_9(AsO_4)_6(H_2O)_4$ (a), the edge sharing Zn polyhedra chain along the [111] (b) and the cluster of As- and Zn-tetrahedra (c). 57
- Figure 15.** Raman spectrum of $Zn_9(AsO_4)_6(H_2O)_4$ 64
- Figure 16.** The sample material with $Cd_{4.65}Ni_{0.35}(H_2O)_4(AsO_4)_2(HAsO_4)_2$ (a) and the single crystal (b, c). Right Image (b) is taken with a light microscope, left image (c) is an BSE-image of $Cd_{4.65}Ni_{0.35}(H_2O)_4(AsO_4)_2(HAsO_4)_2$ 64
- Figure 17.** Image of the structure of $Cd_{4.65}Ni_{0.35}(H_2O)_4(AsO_4)_2(HAsO_4)_2$ along [001] (a) and along [010] (b). The five octahedra are connected by AsO_4 and $HAsO_4$ tetrahedra together with hydrogen bonds. 64
- Figure 18.** Raman spectrum of $Cd_{4.65}Ni_{0.35}(H_2O)_4(AsO_4)_2(HAsO_4)_2$ 73

LIST OF TABLES

Table 1.	A detailed list of the used chemicals.	31
Table 2.	Results of the syntheses.	32
Table 3.	Crystal data, data collection and refinement details for α - and β -(C ₆ H ₁₁ N ₂) ₂ [CdBr ₄].....	35
Table 4.	Crystal data, data collection and refinement details for Zn ₉ (AsO ₄) ₆ (H ₂ O) ₄ and Cd _{4.65} Ni _{0.35} (H ₂ O) ₄ (AsO ₄) ₂ (HASO ₄) ₂	36
Table 5.	The results of the qualitative EDS analysis.	38
Table 6.	Fractional atomic coordinates and displacement parameters for α -(C ₆ H ₁₁ N ₂) ₂ [CdBr ₄]. U_{equiv} according to Fischer and Tillmanns (1988). For the H atoms U_{iso} is shown.	45
Table 7.	Anisotropic displacement parameters for α -(C ₆ H ₁₁ N ₂) ₂ [CdBr ₄] defined as $\exp[-2\pi^2 \sum_{i=1}^3 \sum_{j=1}^3 U_{ij} a_i^* a_j^* h_i h_j]$ according to Fischer and Tillmanns (1988).	46
Table 8.	Selected bond distances (Å) for α -(C ₆ H ₁₁ N ₂) ₂ [CdBr ₄].	46
Table 9.	Selected bond angles (°) for α -(C ₆ H ₁₁ N ₂) ₂ [CdBr ₄].	47
Table 10.	Fractional atomic coordinates and displacement parameters for β -(C ₆ H ₁₁ N ₂) ₂ [CdBr ₄]. U_{equiv} according to Fischer and Tillmanns (1988). For the H atoms U_{iso} is shown.	50
Table 11.	Anisotropic displacement parameters for β -(C ₆ H ₁₁ N ₂) ₂ [CdBr ₄] defined as $\exp[-2\pi^2 \sum_{i=1}^3 \sum_{j=1}^3 U_{ij} a_i^* a_j^* h_i h_j]$ according to Fischer and Tillmanns (1988).	50
Table 12.	Selected bond distances (Å) for β -(C ₆ H ₁₁ N ₂) ₂ [CdBr ₄].	51

Table 13.	Selected bond angles (°) for β -(C ₆ H ₁₁ N ₂) ₂ [CdBr ₄].	51
Table 14.	The most intense peaks of the spectra of α - and β -(C ₆ H ₁₁ N ₂) ₂ [CdBr ₄].	53
Table 15.	Fractional atomic coordinates and displacement parameters for Zn ₉ (AsO ₄) ₆ (H ₂ O) ₄ . U_{equiv} according to Fischer and Tillmanns (1988). For the H atoms U_{iso} is shown.	58
Table 16.	Anisotropic displacement parameters for Zn ₉ (AsO ₄) ₆ (H ₂ O) ₄ defined as $\exp[-2\pi^2 \sum_{i=1}^3 \sum_{j=1}^3 U_{ij} a_i^* a_j^* h_i h_j]$ according to Fischer and Tillmanns (1988).	59
Table 17.	Selected bond distances (Å) for Zn ₉ (AsO ₄) ₆ (H ₂ O) ₄ .	60
Table 18.	Selected bond angles (°) for Zn ₉ (AsO ₄) ₆ (H ₂ O) ₄ .	61
Table 19.	Bond-valences for Zn ₉ (AsO ₄) ₆ (H ₂ O) ₄ calculated after Brese and O'Keeffe (1991) and for hydrogen atoms after Ferraris and Ivaldi (1988).	62
Table 20.	Disorder indices (Baur, 1974) of the Zn-polyhedra and As-tetrahedra in Zn ₉ (AsO ₄) ₆ (H ₂ O) ₄ .	63
Table 21.	Disorder parameters (Robinson et al., 1971; Fleet, 1976) for As-tetrahedra and Zn-polyhedra in Zn ₉ (AsO ₄) ₆ (H ₂ O) ₄ .	63
Table 22.	Fractional atomic coordinates and displacement parameters for Cd _{4.65} Ni _{0.35} (H ₂ O) ₄ (AsO ₄) ₂ (HAsO ₄) ₂ . U_{equiv} according to Fischer and Tillmanns, (1988). For the H atoms U_{iso} is shown.	68
Table 23.	Anisotropic displacement parameters for Cd _{4.65} Ni _{0.35} (H ₂ O) ₄ (AsO ₄) ₂ (HAsO ₄) ₂ defined as $\exp[-2\pi^2 \sum_{i=1}^3 \sum_{j=1}^3 U_{ij} a_i^* a_j^* h_i h_j]$ according to Fischer and Tillmanns (1988).	69
Table 24.	Selected bond distances (Å) for Cd _{4.65} Ni _{0.35} (H ₂ O) ₄ (AsO ₄) ₂ (HAsO ₄) ₂ .	70
Table 25.	Bond valences for Cd _{4.65} Ni _{0.35} (H ₂ O) ₄ (AsO ₄) ₂ (HAsO ₄) ₂ calculated after Brese and O'Keeffe (1991) and for hydrogen atoms after Ferraris and Ivaldi (1988).	70

Table 26.	Selected bond angles (°) for $\text{Cd}_{4.65}\text{Ni}_{0.35}(\text{H}_2\text{O})_4(\text{AsO}_4)_2(\text{HAsO}_4)_2$	71
Table 27.	Disorder indices (Baur, 1974) of the M-octahedra and As-tetrahedra in $\text{Cd}_{4.65}\text{Ni}_{0.35}(\text{H}_2\text{O})_4(\text{AsO}_4)_2(\text{HAsO}_4)_2$	71
Table 28.	Disorder parameters (Robinson et al., 1971; Fleet, 1976) for As-tetrahedra and Zn-polyhedra of $\text{Cd}_{4.65}\text{Ni}_{0.35}(\text{H}_2\text{O})_4(\text{AsO}_4)_2(\text{HAsO}_4)_2$	72

1 INTRODUCTION

1.1 Arsenic

Arsenic is a highly toxic trace element. Humans have been familiar with arsenic for a long time. They used it as poison or curative and for decoration and pigmentation since the Ancient Greeks. Because of its electronic structure and bonding properties it has a broad variety of forms in the solid, aqueous and gas state (O'Day, 2006).

Arsenic has several oxidation states -III, -I, 0, +III, +V. The oxidation states -I, +III and +V are the most common ones in nature. Arsenic with the oxidation state -I is commonly building sulfides in reducing conditions and oxidative weathering is building arsenites (+III) and arsenates (+V) (Reeder et al., 2006). Over 490 minerals (www.mindat.org) contain arsenic as an essential structure component. The most common arsenic minerals are arsenates (Figure 1).

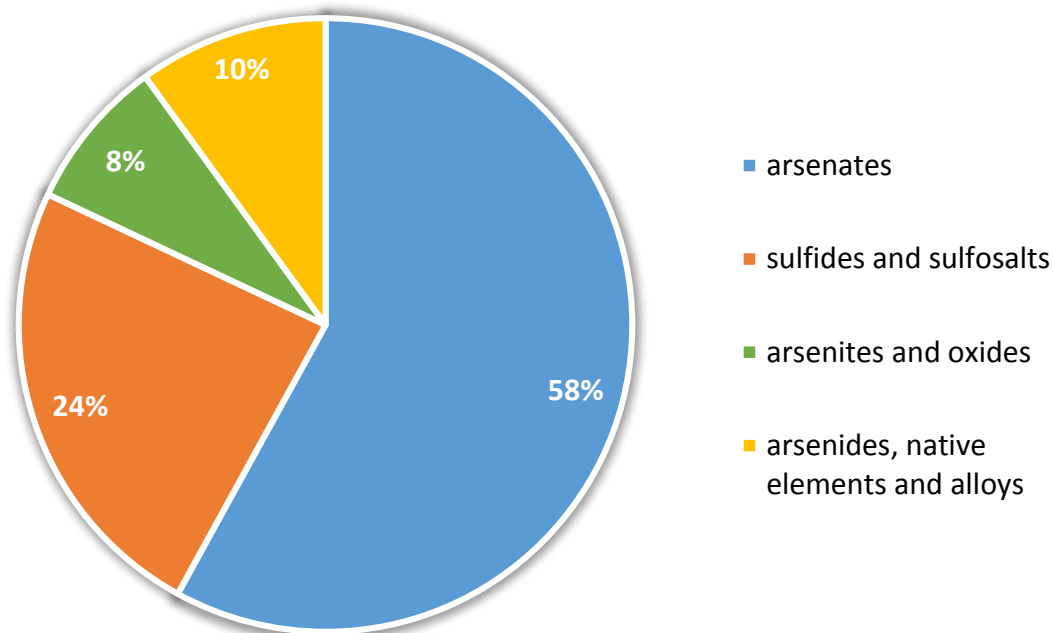


Figure 1. A graphical representation of the distribution of arsenic in minerals according to the data of Strunz and Nickel (2001).

Introduction

Arsenic amount in the earth's crust is about 1.5 ppm (Barbalace, 1995-2016). Contaminations can be caused by natural sources like weathering, biological activity, volcanism or anthropogenic sources (Cullen and Reimer, 1989; Jiang et al., 2013). Common sources of arsenic are mine wastes, tailings ponds and mine drainages. Furthermore, common industrial sources are arsenic-bearing pesticides or herbicides. Also smelting processes or combustion of fossil fuels can produce arsenic-bearing waste (Reeder et al., 2006). Humans can get contaminated with arsenic through ingestion of water and food (Reeder et al., 2006).

1.2 Cadmium

Cadmium is a highly toxic and carcinogenic trace element. It has the atomic number 48 and prefers the oxidation state +II. The concentration in the earth's crust is about 0.11 ppm (Barbalace, 1995-2016). It occurs in nature at low concentrations, often in association with sulphide ores with zinc, lead and copper (Järup, 2003).

Cadmium compounds are used as stabilisers in PVC products and colour pigment. Now the most common usage is in rechargeable nickel-cadmium batteries. Cadmium can also occur in phosphate fertilisers (Järup, 2003) and in mining and smelting processes of lead and zinc as a by-product.

Environmental pollution with cadmium is mainly caused by humans, by combustion of fossil fuels, leachate from landfill sites, run-off from agricultural land and mining residues (Muntau and Baudo, 1992). Contamination of soils with cadmium is a worldwide problem especially for food and drinking water (Taylor et al., 2008).

1.3 Cadmium arsenates

Cadmium and arsenic occur together in smelting operations, metal-arsenic-bearing materials like pesticides or insecticides and mine drainage (Gräfe et al., 2004). Together with other heavy metals they produce different kinds of mine and industrial wastes. One of the main environmental problems is the contamination of water and soils with these wastes and their tendency to chemically react with water producing contaminated water (Nordstrom, 2011). Therefore, technologies have been and still are developed to deal with this problem.

Introduction

A common technique for removing soluble arsenic from water is the precipitation of nearly insoluble arsenic-bearing compounds (Bothe and Brown, 1999). Especially at mine drainages the precipitation of metal-arsenates is important for the immobilisation of arsenic and toxic heavy metals like cadmium (Johnson et al., 2003). If the toxic elements are released or restored depends on the stability of the arsenic-bearing minerals. To investigate the stabilities of these minerals in the environment the synthesis of mineral-related phases can be an appropriate method. It could lead to increased stability of waste bearing phases (Johnson et al., 2003).

2 METHODOLOGY

2.1 Hydrothermal synthesis

“Hydrothermal” is a well-known term in Earth sciences. It describes the reaction of water under elevated temperature and pressure conditions which leads to the formation of various minerals. Hydrothermal techniques can be used to understand the mineral formation in nature. The main part of these techniques is the simulation of natural conditions and synthesising them in the laboratory (Byrappa and Yoshimura, 2013a).

An important hydrothermal technique is the hydrothermal synthesis. In general the hydrothermal synthesis is defined as a heterogeneous reaction that occurs above room temperature and under elevated pressure (> 1 atm) in aqueous solutions in a closed system (Byrappa and Yoshimura, 2013a). Reactants which are difficult to dissolve under normal conditions dissolve by forming complexes under the action of solvents. A solvent like water works as a medium providing a suitable environment. To increase the formation of complexes, mineralisers are used. They are used to catalyse the process. An application of this synthesis method is the production of single crystals of various sizes. The developing of big, pure and dislocation-free single crystals is possible which is advantageous for crystals with specific physical and optical properties (Byrappa and Yoshimura, 2013a).

For crystal growth a pressure vessel capable of containing highly corrosive solvents at high pressure and temperature conditions and building up a closed system is required. Therefore, an autoclave is used. Choosing the right autoclave depends on the conditions of the synthesis. It should be inert to acids, bases and oxidising agents, leak-proof and rugged enough to bear high-pressure and high-temperature experiments for a long duration. If Morey-autoclaves are used (Figure 2), which are metal flat-plate closure autoclaves, the temperature is controlled externally and an autogenous pressure will be generated by the autoclave itself depending on the degree of filling, the fluid and the temperature (Byrappa and Yoshimura, 2013b).

The advantages of the hydrothermal synthesis are the relatively fast growth, the purity and the lack of dislocations of single crystals. The method is also useful to synthesise low



Figure 2. Morey-autoclave with Teflon vessel.

temperature phases and it is also possible to synthesise metastable compounds (Byrappa and Yoshimura, 2013a). Disadvantages of a hydrothermal synthesis are the lack of observability of the crystal growth during the synthesis process and the challenge to find an appropriate autoclave material which depends on the components of the synthesis.

2.2 Ionothermal synthesis

Ionothermal synthesis describes the usage of ionic liquids as solvent and template or structure directing agent simultaneously. The process is similar to the hydrothermal synthesis or other solvothermal syntheses but the used solvents are fundamentally different (Morris, 2009).

2.2.1 Ionic liquids

Ionic liquids are also known as 'molten salts'. According to Wasserscheid and Keim (2000) they have a melting point below 100°C and normally they consist of an organic cation and organic or inorganic anion (Figure 3). Due to the variation of the anions or the length of the alkyl groups the physiochemical properties like viscosity, conductivity, hydrophobicity, melting point, *etc.* are very various. Thus, it is possible to design ionic liquids for a certain application (Moosavi, 2013).

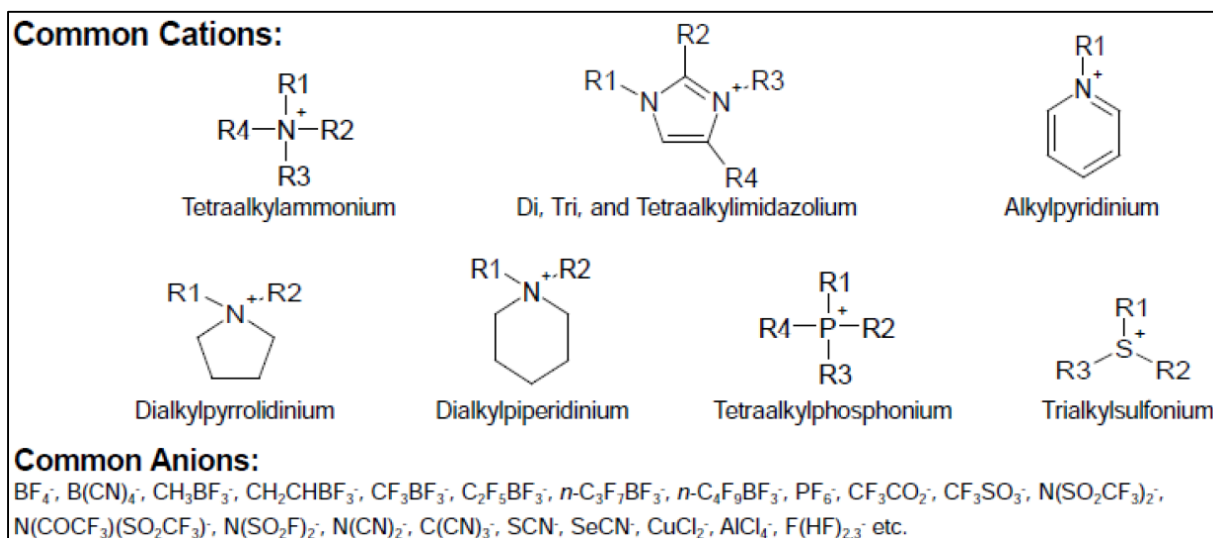


Figure 3. Common cations and anions for ionic liquids (Moosavi, 2013).

In solvothermal synthesis, ionic liquids can be used as solvents, templates and catalysts and they are an excellent alternative to volatile organic solvents (Martínez-Palou, 2010). They are called 'green solvents' because of their low toxicity and the very low vapour pressure. No solvent can get lost through evaporation (Wasserscheid and Keim, 2000). Ionic liquids are also thermally and chemically stable and have non-flammable and non-corrosive properties. Other mentionable profitable properties are the wide electrochemical window, the relatively high electrical conductivity, the high heat capacity, the highly effective interactions with microwave energy and the large range of polarities (Martínez-Palou, 2010; Moosavi, 2013).

Around the 1980s ionic liquids appeared as new reaction media and as catalysts for organic synthesis (Fry and Pienta, 1985). Due to the further developments and the increasing of the different properties over the recent years ionic liquid are used in the inorganic chemistry as well, for example in the synthesis of inorganic materials like molecular sieves (for example Xu et al., 2006 and Liu et al., 2011) or microspheres (for example Cao et al., 2010 and Li et al., 2012). The ionothermal synthesis can be also used for the synthesis of metal-organic frameworks and inorganic-organic hybrids (for example Liao et al., 2006 and Lin et al., 2006). Other important applications of ionic liquids are the separation and extraction of metals (Tian, 2012).

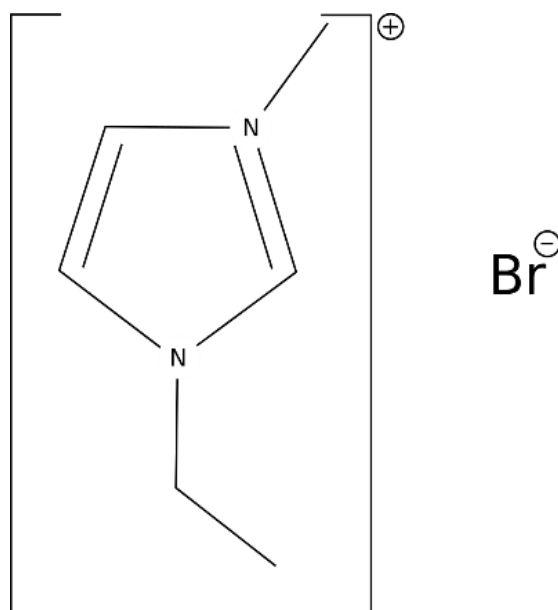


Figure 4. The skeletal formula of 1-ethyl-3-methylimidazoliumbromide.

2.2.1.1 1-Ethyl-3-methyl-imidazolium bromide: [emim]Br

For the Ionothermal synthesis performed within this work 1-ethyl-3-methyl-imidazolium bromide ([emim]Br), $C_6H_{11}N_2Br$, was used. Figure 4 shows the schematic structure of the molecule. The imidazolium ring with an ethyl group on the first position and a methyl group on the third position is positively charged and the bromine is negatively charged.

[Emim]Br has several properties which are profitable for using it as a solvent and template. It has a melting point of $83^{\circ}C$ and a wide liquid range. The vapour pressure is very low. It is profitable for the synthesis in autoclaves and also for microwave synthesis because there is no pressure build up during heating (Wragg et al., 2009). [Emim]Br has also good solvating properties (Anthony et al., 2003) and has a hygroscopic character which means that there is always a small amount of water. Even after a moderate drying process it can contain a small amount of water (Parnham et al., 2007). The decomposition of the liquid takes place at $311.85^{\circ}C$, but the decomposition process starts already slowly at $199.85^{\circ}C$ with CH_3Br and C_2H_5Br as products (Chambreau et al., 2012).

[Emim]Br is often used as a solvent and template in the synthesis of zeolite-like phosphates (e.g. Su et al., 2011), metal-organic frameworks (e.g. Lin et al., 2006) and inorganic-organic hybrids (e.g. Parnham and Morris, 2007; Thirumurugan and Rao, 2008).

2.3 Single crystal X-ray diffraction

Single crystal X-ray diffraction is a non-destructive analytical method for analysing the atom positions in a crystal structure and delivering detailed information about a crystal lattice. The method is based on the discovery of the diffraction of X-rays by crystals. An X-ray beam is diffracted by the crystal if the conditions fulfil the Laue equations.

Usually, the measurement is executed by a four-circle-diffractometer. It has three rotation axes which intersect in one point with an accuracy under 10 μm where the crystal is positioned. On the fourth circle the detector is positioned. A computer controls the rotations and moves the mounted crystal in the right position where the Bragg equation can be fulfilled and the X-ray beam is in reflection position (Kleber et al., 2010). The detector can move to a certain angle and register the intensity of the scattered X-ray beam. Nowadays, an area detector (CCD-detector, Pixel-detector) is used (Massa, 2011).

There are two types of circle system: the Euler geometry and the Kappa geometry. The Euler geometry has an ω -circle which rotates the basis of the χ -circle. The χ -circle is vertical to the ω -circle and the goniometer head is sitting in the inner side of this circle and can also rotate in the ϕ -circle. The θ -circle carries the detector and has the same axis as the ω -circle. In the Kappa geometry the ω -circle and θ -circle are arranged equally to the Euler geometry. The κ -circle replaces the χ -circle and its axis has an angle of 50° to the horizontal plane. The axis of the ϕ -circle has also an angle of 50° to the plane of the κ -circle and rotates the goniometer head. Because of the rotation of the κ - and ϕ -circle the χ -circle of the Euler geometry can be replaced and there is no more need for a physical circle around the crystal (Massa, 2011).

The four-circle-diffractometer can be used for phase identification and intensity measurements. For the phase identification only a few orientation images have to be recorded. After a peak search the orientation matrix and the unit cell have to be determined with an indexing program. With this information the crystal can be identified and the final measurement parameters (crystal-to-detector distance, angle width, step width, exposure time) for the intensity measurement can be chosen. After an intensity measurement the diffraction pattern should be checked and a reflection profile should be determined. Now the

Methodology

intensities have to be integrated. After processing the data and after some corrections (underground, Lorentz-factor, polarisation-factor, absorption) for data reduction the observed structure factors (F_o values) can be produced which are compared to the calculated F_o values (Massa, 2004).

Now the structure can be solved and refined by using a suitable software like the program SHELX (Sheldrick, 2008). The program SHELX uses the direct methods or the Patterson method for the structure solution and afterwards the structure refinement can be started by using the least squares method. During the refinement the R-factor (residual factor) shows how well a structural model actually conforms to reality (Massa, 2004).

2.4 Raman Spectroscopy

The 'Raman effect' is an inelastic scattering process which has been discovered by Sir C.V. Raman in 1921 and published by Raman and Krishnan (1928). It describes a change in the wavelength of light by interaction of a light beam with molecular vibrations (Nasdala et al., 2004).

What happens if a beam of light irradiates a molecule or crystal?

1. For absorption of the light the energy of the incoming photon should correlate to the energy difference between two allowed vibrational levels which is only possible with infrared light. This generates a phonon with the same energy as the photon (Figure 5, sketch 1) (Nasdala et al., 2004).
2. But if visible light hits the molecule or crystal it cannot be absorbed because the photon energy is higher than the energy difference between two allowed vibrational levels. The visible light excites the system to a high-energy state from which the system recovers immediately. So the photon energy of the scattered light will have the same photon energy as the incoming visible light. The scattering is an elastic Rayleigh scattering (Figure 5, sketch 2) (Nasdala et al., 2004).
- 3a. On rare occasions the system gains energy and reaches a higher vibrational state through the excitation of a phonon. The photon energy of the scattered light (Raman scattering) will decrease in relation to the exciting photon. This is called a Stokes type Raman scattering (Figure 5, sketch 3a) (Nasdala et al., 2004).
- 3b. In the case of reaching a lower vibrational state through disexcitation of a phonon, the photon energy of the scattered photon will increase. This scattering is the anti-Stokes type Raman scattering (Figure 5, sketch 3b) (Nasdala et al., 2004).

To achieve an interaction of light with a sample, the sample is irradiated with a monochromatic laser with a defined wavelength (e.g. green with 532 nm, blue with 473 nm and red with 633 nm). The laser light interacts with the sample and the photon energy of the

Methodology

scattered light is measured on a detector. The accomplished spectra consist of the strong Rayleigh line and the weak Raman bands. Because of the energy loss the Stokes type Raman bands are considered in lower wavelengths related to the wavelength of Rayleigh line. The anti-Stokes type Raman bands are considered above the Rayleigh line. For Raman spectra only the Stokes type Raman bands are measured because they have a higher intensity than the anti-Stokes type Raman bands.

A Raman spectrum is a plot of intensity *versus* photon energy. The intensity is relatively weak and expressed in counts per second. The photon energy is usually expressed as relative wavenumber ($\tilde{\nu}$), also called Raman shift. It is the wavenumber difference between the incident light and the scattered light. Therefore, the Rayleigh line is set at zero Raman shift and the Stokes type Raman bands have a positive Raman shift. The Raman bands are defined by their location, their relative intensities, their widths (FWHM = full width at half band maximum intensity) and their polarisation. Due to the definition of the Raman bands they are specific for a certain type of sample and they can be used for sample identification (Nasdala et al., 2004).

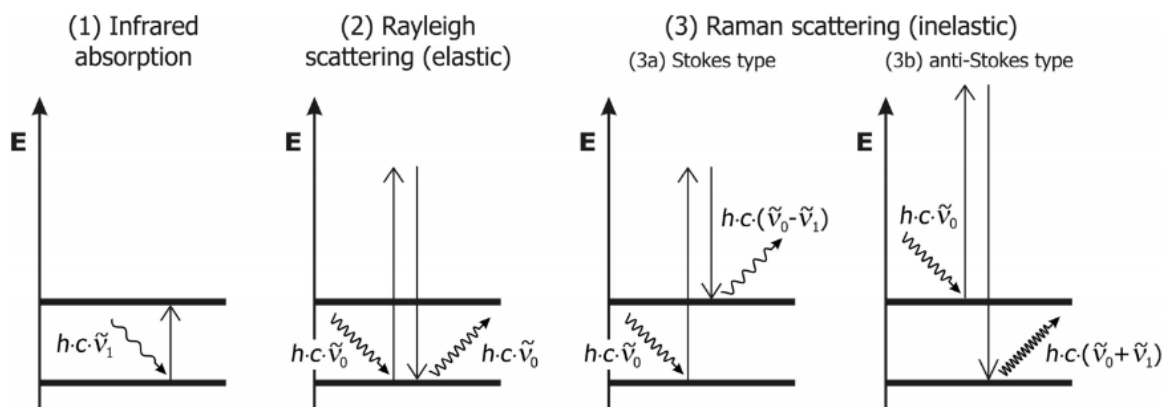


Figure 5. Simplified energy level diagrams which describe the difference between Infrared absorption (1), Rayleigh scattering (2) and Raman scattering (3) (Nasdala et al., 2004).

2.5 Infrared Spectroscopy

Infrared spectroscopy (IR-spectroscopy) is a vibrational spectroscopy method to analyse crystals by stimulation of atoms with IR-light. The vibrating atomic groups interact with the electromagnetic field of the light but only with light that carries the right amount of energy which can lift the atomic groups from one energy level to another, in other words the vibrations of the light and vibrations of the sample must have the same frequency to be IR-active. So the IR radiation can be absorbed and shown in an absorption spectrum (Beran et al., 2004).

On the x-axis of the spectrum the wavenumber is plotted and on the y-axis the transmittance (T) or absorbance (A). Transmittance is without dimension (multiplied by 100 and expressed in [%]) and is defined as the ratio between the intensity of the light after passing the sample (I) and the intensity of the incident light (I_0). I_0 can be determined from a background spectrum collected from an empty sample holder or with an IR-inert material such as KBr.

$$T = I/I_0$$

The intensities are related to the absorbance (A) and defined as the negative common logarithm of T . A is without dimension (expressed as $[\text{cm}^{-1}]$ if measured as an integrated quantity) and according to the Lambert-Beer's law it has a linear relation to the absorption coefficient (a) with the concentration (c) of an absorber. The scaling factor ε is the molar absorption coefficient. (Libowitzky and Beran, 2004).

$$A = -\log(T) \rightarrow A = at \rightarrow a = \varepsilon c$$

An IR-spectrometer may have two different construction types: the non-dispersive IR-spectrometer with no variable wavelength selection and the dispersive and Fourier-Transform-IR-Spectrometer with variable wavelength selection. The dispersive spectrometer has a monochromator for variable wavelength selection and the sample chamber is in front of it. The FTIR-Spectrometer has an interferometer for variable wavelength selection and the sample chamber is after it (Günzler and Heise, 1996).

Methodology

The nondispersive spectrometer has filters for the observation of certain wavelengths. Often used for H₂O/CO₂ amount determination (Günzler and Heise, 1996).

Construction of a dispersive spectrometer: a beam of polychromatic infrared light is emitted from an IR-source and with rotating mirrors the beam is split in two equivalent parts, the measuring beam and the reference beam. The measuring beam which is travelling through the sample gets partly absorbed by interaction with characteristic vibration of the sample. The reference beam has no absorption. So the difference between the beams can be plotted as absorption bands (Günzler and Heise, 1996). Then, the beam can be modulated in energy with a grid monochromator (Libowitzky and Beran, 2004).

Construction of a FTIR-Spectrometer: the main part is the interferometer. The beam of polychromatic infrared light is split in two parts by a beam splitter. One part gets reflected on a moving mirror and the other part on a fixed mirror and after recombination the beam is brought to interference. Because of the shift of the movable mirror a phase difference occur. The now produced interferogram is undergoing a Fourier-Transformation which converts the signals into an absorbance spectrum (Günzler and Heise, 1996).

The sample preparation can be very difficult. The absorbance is proportional to the thickness of the sample. So the intensity of the bands can be affected by the thickness of the sample. (Günzler and Heise, 1996). If enough sample material is available pellets with KBr can be produced. Another possibility to measure the sample is using transparent single crystals. Therefore a microscope with slits must be used. In both cases the sample material must be very clean.

2.6 Scattered electron microscopy

A scanning electron microscope (SEM) is one of the multi-functional methods for the analysis of microstructural characteristics of solid materials because of its high instrumental resolution (in the order of 1-5nm) and its large depth of field, which is responsible for the three-dimensional appearance of the analysed material. It is also possible to analyse material at very low magnification. The SEM image can be used to complement structural and chemical information which is already available from other analytical methods (light microscope, X-ray diffraction, etc.) (Goldstein et al., 2003).

The basic components are the electron column with the electron gun, the lenses, the deflection system and the electron detector, the visual and photorecording cathode ray tubes (CRTs), and the connected electronics. Figure 6 shows a schematic diagram of an electron column. The electron gun generates electrons and accelerates them to an energy in the range of 0.1-30 keV. Electron lenses are used to demagnify the large electron beam from the gun and produce a small electron beam on the sample material. Depending on the quality of the SEM an electron beam with a spot size less than 10nm can be produced. To get an image of the sample material the beam has to move. Two pairs of electromagnetic deflection coils (scan coils) are used to move the beam over the sample surface (Goldstein et al., 2003).

Because of the interaction of the accelerated and focused electrons with the sample material a variety of different signals can be detected. The two imaging signals are the secondary electrons (SE) and the backscattered electrons (BSE). The secondary electrons are generated only in a volume extending a few nanometres from the surface into the sample due to their low energy. They are capable of carrying information about the topography and fine-scale surface texture of the sample material. Backscattered electrons have a higher energy than secondary electrons and thus penetrate farther into the sample. Primary electrons have undergone numerous elastic scattering events to accumulate enough deviation to escape from the sample as BSE. The intensity of the BSE signal depends on the atomic number. Backscattering increases with an increasing atomic number. So the BSE signal carries information about the composition of the material (Goldstein et al., 2003).

Methodology

The electron beam also generates characteristic X-rays, which can be used for chemical analysis. An energy-dispersive X-ray spectrometer (EDS) can detect and measure the X-rays and convert them into a useful form for qualitative analysis. The most common X-ray detector is the lithium-drifted silicon Si(Li) solid state detector (Goldstein et al., 2003). Other types of signals caused by the interaction of the electron beam with the sample material are Auger electrons and cathodoluminescence.

The samples have to be electrically conductive. Single crystals were mounted on adhesive metal foil and coated with carbon. To avoid contamination of the sample chamber of the SEM it is necessary that every crystal is fixed.

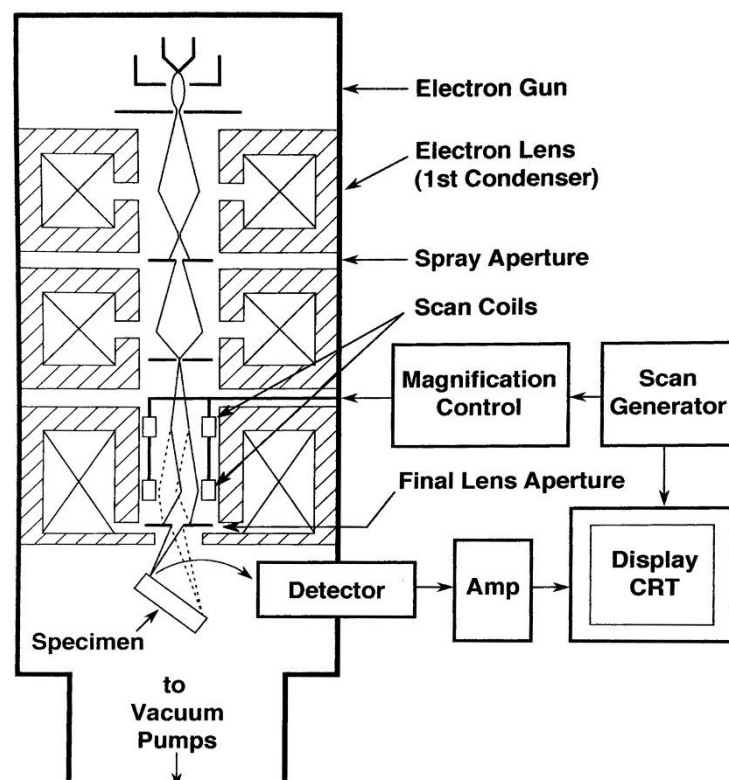


Figure 6. A schematic diagram of an electron column (Goldstein et al., 2003).

3 EXPERIMENTAL

3.1 Synthesis of the single crystals

Within this work, four synthesis runs under different temperature conditions were performed. The temperature gradient during the synthesis was equal in all four synthesis cycles for comparable results (Figure 7).

The starting reagents were chosen after the system $\text{CdO-MO-As}_2\text{O}_5\text{-IL/H}_2\text{O}$ with $M = \text{Mg}^{2+}$, Mn^{2+} , Ni^{2+} , Zn^{2+} (Table 1). The chemicals were mixed together and placed in autoclaves lined with Teflon vessels. The Teflon vessels were filled to 70-90% with the starting mixture and the solvent (distilled water or the ionic liquid [emim]Br). For the mixtures with water as solvent the pH values were noted.

The autoclaves were heated up under autogenous pressure in the Heraeus T6030-drying chamber. The syntheses were running for one week. They were heated up for 4 hours from room temperature to the maximum temperature (220°C, 160°C, 140°C, 120°C) and this temperature was held for 3 days (72 h). After a cooling phase of 99 hours the syntheses were finished (Figure 7). The reaction products were usually washed thoroughly with water or ethanol, filtered and dried at room temperature.

Table 1. A detailed list of the used chemicals.

name	purity	producer	amount
[emim] Br	dry, $\geq 98.5\%$ (HPLC/T)	Fluka	25 g
[emim] Br	$\geq 97,0\%$ (T)	Fluka	50 g
As_2O_5	99.9 % (metal basis)	Alfa Aesar	25 g
CdO	Assay $\geq 99\%$ (KT)	Fluka	100 g
$\text{Mg}(\text{OH})_2$	Assay $\geq 99\%$ (KT)	Fluka	250 g
$\text{Mn}(\text{NO}_3)_2 \cdot x\text{H}_2\text{O}$	98%	Sigma-Aldrich	500 g
$\text{Ni}(\text{OH})_2$	-	Sigma-Aldrich	250 g
$\text{Zn}(\text{NO}_3)_2 \cdot 6\text{H}_2\text{O}$	reagent Grade, 98%	Sigma-Aldrich	500 g

Experimental

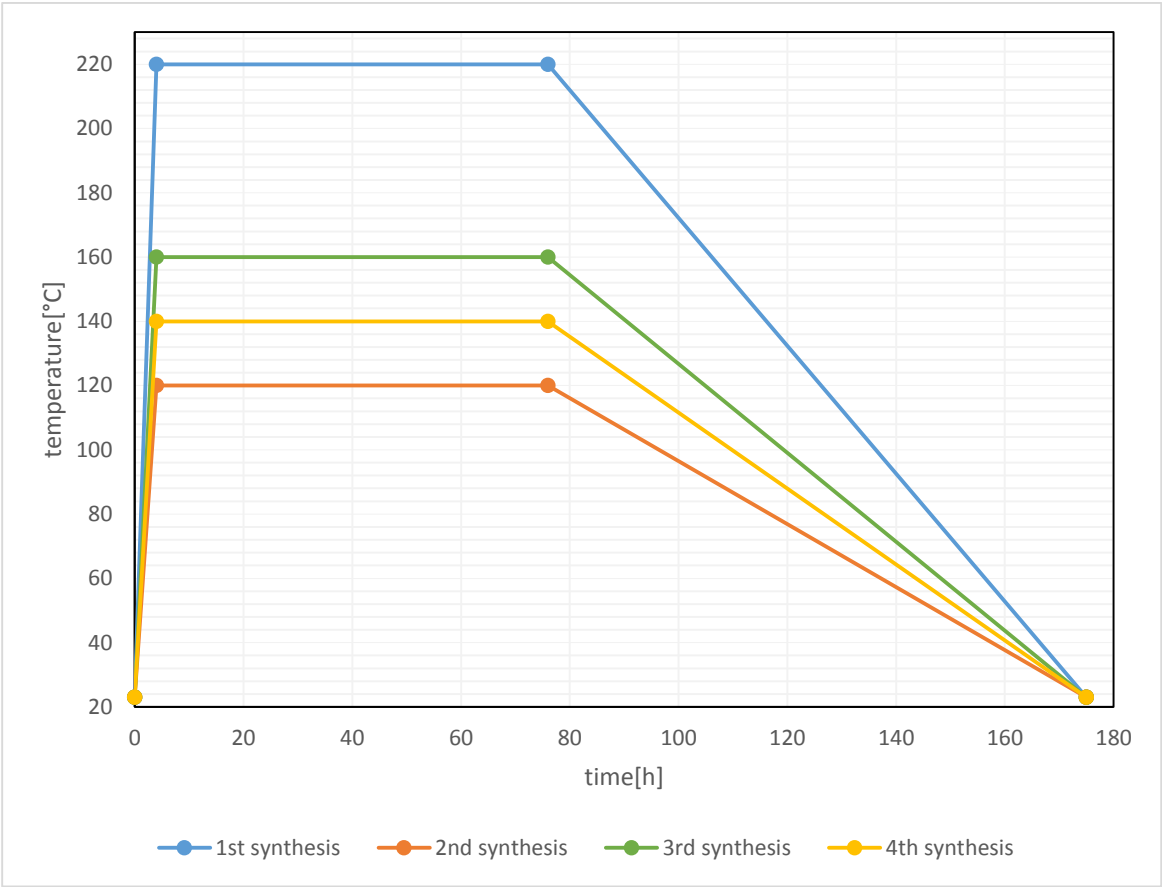


Figure 7. Temperature gradient for the four synthesis cycles.

Experimental

Table 2. Results of the syntheses in the system CdO–MO–As₂O₅–(H₂O/IL).

hydrothermal synthesis		
max. temp.	sample no.	crystals with single crystal X-ray diffraction quality
120°C		
	A2o	Cd _{4.65} Ni _{0.35} (H ₂ O) ₄ (AsO ₄) ₂ (HAsO ₄) ₂
	A3o	Mn ₅ (AsO ₄) ₂ (HAsO ₄) ₂ ·4H ₂ O (Stock et al., 2002)
140°C		
	A1o	Mg ₂ (OH)(AsO ₄) (Rojo et al., 1997)
	A3o	Cu ₂ (AsO ₄)(OH) (Olivenite)
	A4o	Zn ₂ (AsO ₄)(OH) (Adamite)
220°C		
	A1o	Mg _{6.75} (OH) ₃ (H _{0.166} AsO ₄) ₃ (HAsO ₄) (Weil, 2013)
	A1o	Mg ₂ (OH)AsO ₄ (Rojo et al., 1997)
	A3o	Mn ₅ (AsO ₄) ₂ (HAsO ₄) ₂ ·4H ₂ O (Stock et al., 2002)
ionothermal synthesis		
max. temp.	sample no.	crystals with single crystal X-ray diffraction quality
120°C		
	A1u	α-(C ₆ H ₁₁ N ₂) ₂ [CdBr ₄]
	A2u	α-(C ₆ H ₁₁ N ₂) ₂ [CdBr ₄]
	A3u	α-(C ₆ H ₁₁ N ₂) ₂ [CdBr ₄]
140°C		
	A1u	α-(C ₆ H ₁₁ N ₂) ₂ [CdBr ₄]
	A2u	α-(C ₆ H ₁₁ N ₂) ₂ [CdBr ₄]
	A4u	Zn ₉ (AsO ₄) ₃ (H ₂ O) ₄ (Feng et al., 1997; Jensen et al., 1998)
	A4u	Zn ₂ (AsO ₄)(OH) (Adamite)
160°C		
	A2u	α-(C ₆ H ₁₁ N ₂) ₂ [CdBr ₄]
	A3u	α-(C ₆ H ₁₁ N ₂) ₂ [CdBr ₄]
	T2	α-(C ₆ H ₁₁ N ₂) ₂ [CdBr ₄]
	T2	Zn ₉ (AsO ₄) ₃ (H ₂ O) ₄ (Feng et al., 1997; Jensen et al., 1998)
	T2	Zn ₂ (AsO ₄)(OH) (Adamite)
220°C		
	A1u	β-(C ₆ H ₁₁ N ₂) ₂ [CdBr ₄]
	A3u	β-(C ₆ H ₁₁ N ₂) ₂ [CdBr ₄]

3.2 Single crystal X-ray diffraction measurements

The raw-intensity data for α -(C₆H₁₁N₂)₂[CdBr₄], Zn₉(AsO₄)₆(H₂O)₄ and Cd_{4.65}Ni_{0.35}(H₂O)₄(AsO₄)₂(HAsO₄)₂ were collected on a Nonius Kappa CCD single-crystal four-circle diffractometer and the intensity data for β -(C₆H₁₁N₂)₂[CdBr₄] were collected with a Bruker X8 Kappa APEX II CCD. Both diffractometers are constructed with four circles with κ -geometry, are equipped with capillary-optics collimators and CCD area detectors and used graphite monochromated MoK α radiation ($\lambda = 0.70926 \text{ \AA}$).

At the Nonius Kappa the following programs were used: HKL SCALEPACK (Nonius, 2005-2007) for determination of the unit-cell parameter, DENZO-SMN (Nonius, 2005-2007) for processing of the intensity data, and the multi-scan method (Otwinowski et al., 2003) for absorption corrections. For determination and refinement of the unit-cell, the processing of the data and data corrections at the Bruker diffractometer, a Bruker APEX software suite (Bruker, 2007) was used. The intensity data and all measurement parameters are listed in Table 3 and Table 4. The structures were solved with direct methods and refined by a full-matrix least-squares procedure based on F^2 with SHELXL 2013 (Sheldrick, 2008) and winGX (Farrugia, 2012). For the refinement of Cd_{4.65}Ni_{0.35}(H₂O)₄(AsO₄)₂(HAsO₄)₂ the atom positions of the mineral Miguelromeroite (Kampf, 2009) were used and for Zn₉(AsO₄)₆(H₂O)₄ the atom positions of Zn₉(AsO₄)₆·4(H₂O) (Jensen et al., 1998) were used. For all crystals all atoms except hydrogen were refined anisotropically. The hydrogen atoms are determined in the Fourier map and are isotropically refined. Hydrogen atoms from hydroxyl groups and water molecules in Zn₉(AsO₄)₆(H₂O)₄ and Cd_{4.65}Ni_{0.35}(H₂O)₄(AsO₄)₂(HAsO₄)₂ were placed in geometrically calculated positions and refined using fixed distances and displacement parameters: O–H=0.82 Å and $U_{\text{iso}}(\text{H})=1.2U_{\text{eq}}(\text{O})$ for hydroxyl groups and O–H=0.85 Å and $U_{\text{iso}}(\text{H})=1.2U_{\text{eq}}(\text{O})$ for water molecules. The hydrogen atoms in α - and β -(C₆H₁₁N₂)₂[CdBr₄] are refined after crystallographic standards for aromatic and aliphatic hydrogen atoms also using fixed distances and displacement parameters: for the methyl H-atoms C–H=0.96 Å and $U_{\text{iso}}(\text{H})=1.5U_{\text{eq}}(\text{C})$, for the methylene H-atoms C–H=0.97 Å and $U_{\text{iso}}(\text{H})=1.2U_{\text{eq}}(\text{C})$ and for the imidazolium ring H-atoms C–H = 0.93 Å and $U_{\text{iso}}(\text{H})=1.2U_{\text{eq}}(\text{C})$. All details were listed in Table 3 and Table 4 and the visualisation of the structures was performed with the program ATOMS (Dowty, 2006).

Experimental

Table 3. Crystal data, data collection and refinement details for α - and β -(C₆H₁₁N₂)₂[CdBr₄].

Crystal data	α -(C ₆ H ₁₁ N ₂) ₂ [CdBr ₄]	β -(C ₆ H ₁₁ N ₂) ₂ [CdBr ₄]
Chemical formula	C ₁₂ H ₂₂ Br ₄ CdN ₄	C ₁₂ H ₂₂ Br ₄ CdN ₄
Formula weight, M_r (g/mol)	654.37	654.37
Space group (Nr.)	$P2_1/c$ (Nr.14)	$I4_1/a$ (Nr.88)
a [Å]	13.975(3)	14.863(2)
b [Å]	10.343(2)	14.863(2)
c [Å]	14.895(3)	20.600(4)
α [°]	90	90
β [°]	94.35(3)	90
γ [°]	90	90
V [Å ³]	2146.8(8)	4550.9(16)
Z	4	8
Crystal size (mm)	0.01 × 0.02 × 0.25	0.01 × 0.02 × 0.15
Absorption coefficient, μ (mm ⁻¹)	8.46	7.98
T_{\min} / T_{\max}	0.816/0.929	0.826/0.932
$F(000)$, ρ_{calc} [g/cm ³]	1240, 2.025	2480, 1.910
Data collection		
Crystal-detector distance (mm)	40	40
Rotation width (°)	2	2
$2\vartheta_{\max}$ [°]	70	50
Total no. of frames	659	817
Collection time per frame (s)	100	300
h_{\min}/h_{\max}	-18/18	-17/17
k_{\min}/k_{\max}	-13/13	-17/17
l_{\min}/l_{\max}	-19/19	-24/24
Absorption correction	Multi-scan	Multi-scan
Reflections collected/unique	9579/4927	39283/2085
Observed reflections [$I > 2\sigma(I)$]	3165	1411
R_{int}	0.032	0.052
Refinement		
Extinction coefficient, k^1	—	—
Refined parameters	190	95
R_1 [$I > 2\sigma(I)$]	0.0326	0.0389
wR_2^b [$I > 2\sigma(I)$]	0.0534	0.0858
R_1 (all)	0.0712	0.0695
wR_2^a (all)	0.0604	0.0995
Goodness-of-fit, S	1.009	1.017
$(\Delta/\sigma)_{\max}$	0.000	0.000
$(\Delta\rho)_{\max} / (\Delta\rho)_{\min}$ [e/Å ³]	0.577/-0.445	0.739/-0.517

¹ $F_c^* = k F_c [1 + 0.001 \times F_c^2 \lambda^3 / \sin(2\theta)]^{-1/4}$

^b $w = 1/[(\sigma^2 F_o^2) + (0.0231 P)^2]$, where $P = (F_o^2 + 2 F_c^2)/3$ for α -(C₆H₁₁N₂)₂[CdBr₄] and $w = 1/[(\sigma^2 F_o^2) + (0.0368 P)^2]$, where $P = (F_o^2 + 2 F_c^2)/3$ for β -(C₆H₁₁N₂)₂[CdBr₄]

Experimental

Table 4. Crystal data, data collection and refinement details for $\text{Zn}_9(\text{AsO}_4)_6(\text{H}_2\text{O})_4$ and $\text{Cd}_{4.65}\text{Ni}_{0.35}(\text{H}_2\text{O})_4(\text{AsO}_4)_2(\text{HASO}_4)_2$.

Crystal data	$\text{Zn}_9(\text{AsO}_4)_6(\text{H}_2\text{O})_4$	$\text{Cd}_{4.65}\text{Ni}_{0.35}(\text{H}_2\text{O})_4(\text{AsO}_4)_2(\text{HASO}_4)_2$
Chemical formula	$\text{H}_8\text{As}_6\text{O}_{28}\text{Zn}_9$	$\text{H}_{10}\text{As}_4\text{Cd}_{4.65}\text{Ni}_{0.35}\text{O}_{20}$
Formula weight, M_r (g/mol)	255.09	1173.10
Space group (Nr.)	$P\bar{1}$ (Nr.2)	$C2/c$ (Nr.15)
a [Å]	6.6983(13)	18.375(4)
b [Å]	9.1885(18)	9.5395(19)
c [Å]	10.146(2)	9.977(2)
α [°]	69.44(3)	90
β [°]	77.26(3)	96.19(3)
γ [°]	75.78(3)	90
V [Å ³]	560.6(2)	1738.6(6)
Z	1	4
Crystal size (mm)	0.03×0.04×0.22	0.02 × 0.02 × 0.10
Absorption coefficient, μ (mm ⁻¹)	18.37	13.63
T_{\min} / T_{\max}	0.418/0.576	0.728/0.761
$F(000)$, ρ_{calc} [g/cm ³]	700, 4.425	2140, 4.482
Data collection		
Crystal-detector distance (mm)	30	30
Rotation width (°)	2	2
$2\theta_{\max}$ [°]	70	70
Total no. of frames	568	545
Collection time per frame (s)	55	150
h_{\min}/h_{\max}	-10/10	-25/26
k_{\min}/k_{\max}	-14/14	-13/13
l_{\min}/l_{\max}	-16/16	-14/14
Absorption correction	Multi-scan	Multi-scan
Reflections collected/unique	9603/4876	5182/2664
Observed reflections [$I > 2\sigma(I)$]	3914	2033
R_{int}	0.031	0.032
Refinement		
Extinction coefficient, k^1	0.0016(3)	—
Refined parameters	208	133
Number of restraints	4	0
R_1 [$I > 2\sigma(I)$]	0.0287	0.0295
wR_2^b [$I > 2\sigma(I)$]	0.0637	0.0585
R_1 (all)	0.0431	0.0508
wR_2^a (all)	0.0681	0.0537
Goodness-of-fit, S	1.023	1.023
$(\Delta/\sigma)_{\max}$	0.001	0.001
$(\Delta\rho)_{\max} / (\Delta\rho)_{\min}$ [e/Å ³]	1.026/-1.276	1.072/-1.073

¹ $F_c^* = k F_c [1 + 0.001 \times F_c^2 \lambda^3 / \sin(2\theta)]^{-1/4}$

^b $w = 1/[(\sigma^2 F_o^2) + (0.0344 P)^2]$, where $P = (F_o^2 + 2 F_c^2)/3$ for $\text{Zn}_9(\text{AsO}_4)_6(\text{H}_2\text{O})_4$ and $w = 1/[(\sigma^2 F_o^2) + (0.0216 P)^2 + 10.3000 P]$, where $P = (F_o^2 + 2 F_c^2)/3$ for $\text{Cd}_{4.65}\text{Ni}_{0.35}(\text{H}_2\text{O})_4(\text{AsO}_4)_2(\text{HASO}_4)_2$

3.3 Raman spectroscopy

For the measurement of the single crystal Raman spectra of $\text{Zn}_9(\text{AsO}_4)_6(\text{H}_2\text{O})_4$ and $\text{Cd}_{4.65}\text{Ni}_{0.35}(\text{H}_2\text{O})_4(\text{AsO}_4)_2(\text{HAsO}_4)_2$ a Horiba LabRAM HR Evolution was used. The system is equipped with a Peltier-cooled CCD detector with a spectral range of 4000 - 60 cm^{-1} and linked with the optical Olympus BX41 Mikroskop equipped with a confocal path of light. The spectra were excited with 633 nm of a He-Ne ion laser. An objective with a magnification of 50 diameters (numerical aperture 0.9) was used to focus the laser beam on the single crystals. Randomly orientated single crystals were measured in the spectral range from 60 to 4000 cm^{-1} . Furthermore an Olympus grating with 1800 lines per mm was used. The nominal exposure time amounts 2×5 s, the lateral resolution is 1.5 μm and the depth resolution is approximately 3 μm .

3.4 Infrared spectroscopy

For the measurement of the Fourier-transform infrared (FTIR) spectra of α - and β - $(\text{C}_6\text{H}_{11}\text{N}_2)_2[\text{CdBr}_4]$ a Bruker Tensor 27 FTIR spectrometer was used. The spectrometer is equipped with a mid-IR Globar light source and KBr beam splitter and is attached to a Hyperion microscope with an MCT-detector. The microscope itself is equipped with a cassegrain-objective with a 15 fold magnification (numeric aperture 0.4) and with two slits. The slits can be adjusted by hand and they are used to concentrate the incoming IR-beam on a specific area on the sample. For α - $(\text{C}_6\text{H}_{11}\text{N}_2)_2[\text{CdBr}_4]$ only the upper slit was used and adjusted to approximately 40 μm . For β - $(\text{C}_6\text{H}_{11}\text{N}_2)_2[\text{CdBr}_4]$ the upper and lower slits were used and the upper slit was adjusted to approximately 20 μm . To get the finished spectra of α - $(\text{C}_6\text{H}_{11}\text{N}_2)_2[\text{CdBr}_4]$ 32 scans were executed, for β - $(\text{C}_6\text{H}_{11}\text{N}_2)_2[\text{CdBr}_4]$ 128 scans were executed. Both spectra were measured in the spectral range of 400 to 4000 cm^{-1} with a resolution of 4 cm^{-1} .

3.5 Scanning electron microscopy/energy dispersive spectroscopy

For the elemental analysis of the four samples the JEOL JSM-6610 LV scanning electron microscope (SEM) at the Natural History Museum in Vienna was used. The SEM is equipped with a thermoionic tungsten filament emitter, SE- and BSE-detectors, an EDS system and EBSD and cathodoluminescence detectors. The single crystals were prepared on a carbon tape attached to an aluminium sample holder and analysed under high vacuum using 15kV accelerating voltage and an accumulation time of 20s. The results of the EDS analysis are listed in Table 5.

Table 5. The results of the qualitative EDS analysis.

sample		Cd	Ni	Zn	As	O	Br	N
α -(C ₆ H ₁₁ N ₂) ₂ [CdBr ₄] [*]	1	10.65	-	-	-	14.70	45.30	29.35
	2	12.46	-	-	-	11.60	46.26	29.68
β -(C ₆ H ₁₁ N ₂) ₂ [CdBr ₄] [*]	1	13.43	-	-	-	9.98	59.84	16.76
Zn ₉ (AsO ₄) ₆ ·4H ₂ O]	1	-	-	20.50	13.17	66.32	-	-
	2	-	-	21.59	13.83	64.58	-	-
Cd _{4.75} Ni _{0.25} (AsO ₄) ₂ (HAsO ₄) ₂ ·4H ₂ O	1	10.30	3.14	-	12.27	74.30	-	-
	2	10.79	2.80	-	10.35	76.05	-	-

^{*} The O content is due to the adsorption of water on the surface of (C₆H₁₁N₂)₂[CdBr₄]

4 RESULTS

4.1 Results of the synthesis

Overall 33 synthesis experiments in the system $\text{CdO}-\text{MO}-\text{As}_2\text{O}_5-(\text{H}_2\text{O}/\text{IL})$ were carried out, one half of them with [emim]Br and the other half with H_2O as solvent. During the synthesis experiments 22 single crystals of good quality for single crystal X-ray diffraction measurement were established (Table 2).

Because of the natural formation of arsenates by weathering of primary ores or by hydrothermal processes, hydrothermal synthesis is a common method to synthesise arsenates. H_2O as the major transporting agent during the hydrothermal synthesis also plays an important part and indeed crystals with the highest quality occurred by using a large amount of water (filling volume of the Teflon vessel 70-90 %) and in samples with moderate pH values (pH=3-6). A new compound, the mineral-like structure, $\text{Cd}_{4.65}\text{Ni}_{0.35}(\text{H}_2\text{O})_4(\text{AsO}_4)_2(\text{HAsO}_4)_2$, was synthesised under hydrothermal conditions.

In the trial ionothermal synthesis in the system $\text{CdO}-\text{ZnO}-\text{As}_2\text{O}_5$, the ionic liquid [emim]Br was tested as solvent and template for arsenate synthesis. [Emim]Br acts as the solvent and template for the two polymorphs of $(\text{C}_6\text{H}_{11}\text{N}_2)_2[\text{CdBr}_4]$, α - and β - $(\text{C}_6\text{H}_{11}\text{N}_2)_2[\text{CdBr}_4]$. The monoclinic polymorph was established in 8 different samples synthesised at 120°C, 140°C and 160°C and the tetragonal polymorph crystallised during only one synthesis run at 220°C in two different samples. Because of the hygroscopic character (Wragg et al., 2009), [emim]Br is not as thermally stable as other ionic liquids. Above 220°C [emim]Br is not stable anymore and decomposes.

Furthermore $\text{Zn}_9(\text{AsO}_4)_6(\text{H}_2\text{O})_4$ (Feng et al., 1997; Jensen et al., 1998) was synthesised in the system $\text{CdO}-\text{ZnO}-\text{As}_2\text{O}_5$ using [emim]Br as solvent at 140°C. The structure of $\text{Zn}_9(\text{AsO}_4)_6(\text{H}_2\text{O})_4$ is already known but was for the first time synthesised using ionothermal synthesis. It was re-refined and the position of the hydrogen atoms was determined for the first time. Besides $\text{Zn}_9(\text{AsO}_4)_6(\text{H}_2\text{O})_4$, the same synthesis product yielded synthetic adamite, $\text{Zn}_2(\text{AsO}_4)(\text{OH})$ and α - $(\text{C}_6\text{H}_{11}\text{N}_2)_2[\text{CdBr}_4]$.

Results

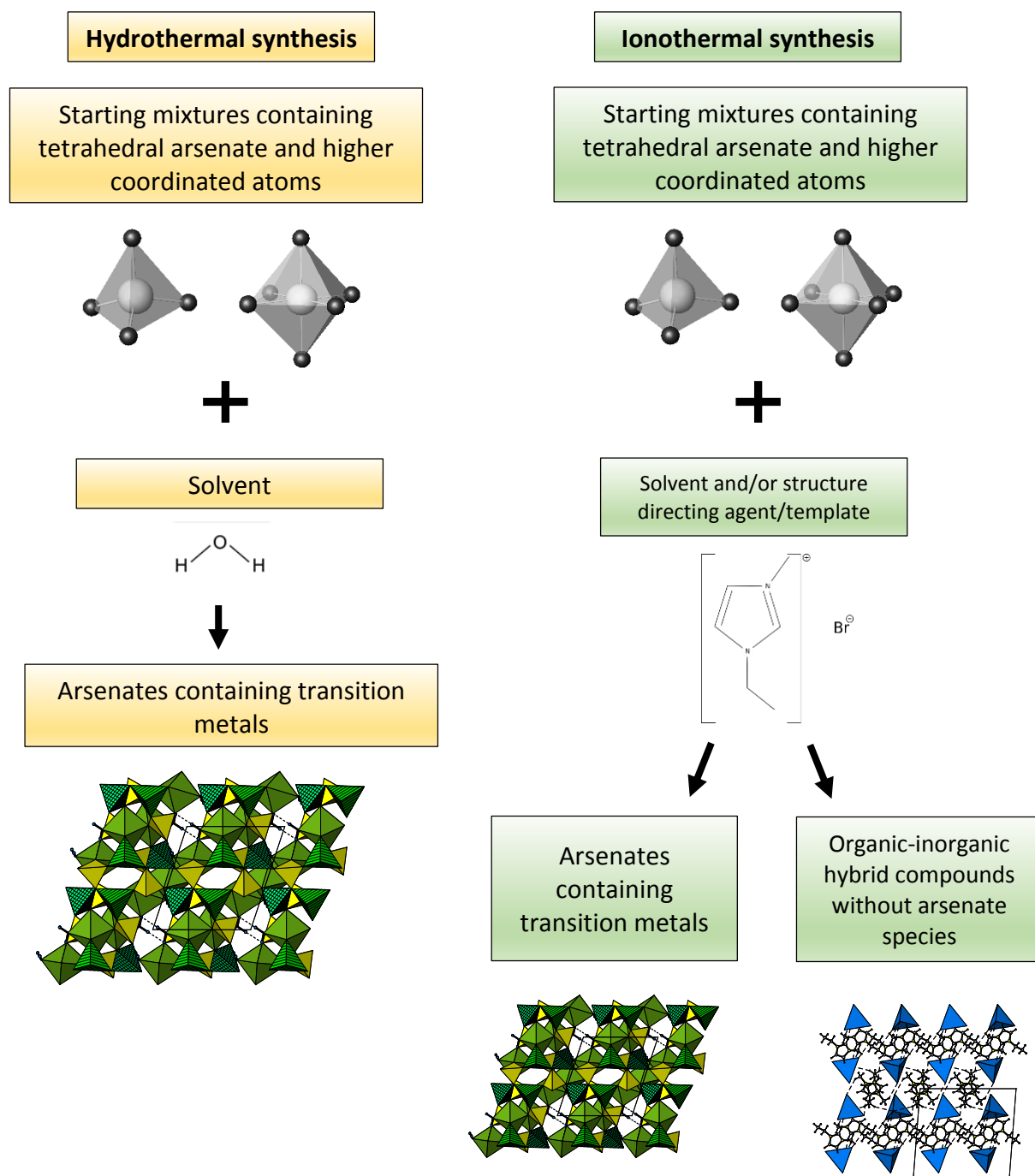


Figure 8. A schematic illustration of the synthesis of tetrahedral-octahedral frameworks under hydrothermal (left) and ionothermal (right) conditions.

4.2 α - and β -(C₆H₁₁N₂)₂[CdBr₄]

1-ethyl-3-methylimidazoliumbromide used as a solvent has separated cadmium from the mixture. The separated cadmium has built up a new organic-inorganic hybrid compound with [emim]Br as template: a 1-ethyl-3-methylimidazolium tetrabromocadmiate. This new complex crystallised in two polymorphic modifications which are differentiated in the conformation and relative orientation of the [C₆H₁₁N₂]⁺ cations and the [CdBr₄]²⁻ anions, combined with different unit cells and space group symmetry. The polymorph occurred as a tetragonal structure, β -(C₆H₁₁N₂)₂[CdBr₄], at 220°C and as a monoclinic structure, α -(C₆H₁₁N₂)₂[CdBr₄], at 160°C and lower synthesis temperatures.

The amount of the tetragonal crystals which were big enough for single crystal measurements was very small and the size of a single crystal was below 0.3 mm. On the other hand, there is an abundant amount of the monoclinic crystals. They appear in 11 different end-products of the synthesis. The crystal size is very variable and goes up to several millimetres.

The SEM-EDS study confirms the presence of Cd, Br and N (Table 5). It also shows small amounts of manganese arsenates in α -(C₆H₁₁N₂)₂[CdBr₄] and cadmium-manganese arsenates in β -(C₆H₁₁N₂)₂[CdBr₄]. They occur as small needle-like crystals with a size of 15 μ m overgrown with the crystals of α - and β -(C₆H₁₁N₂)₂[CdBr₄] (Figure 9e and f).

Results

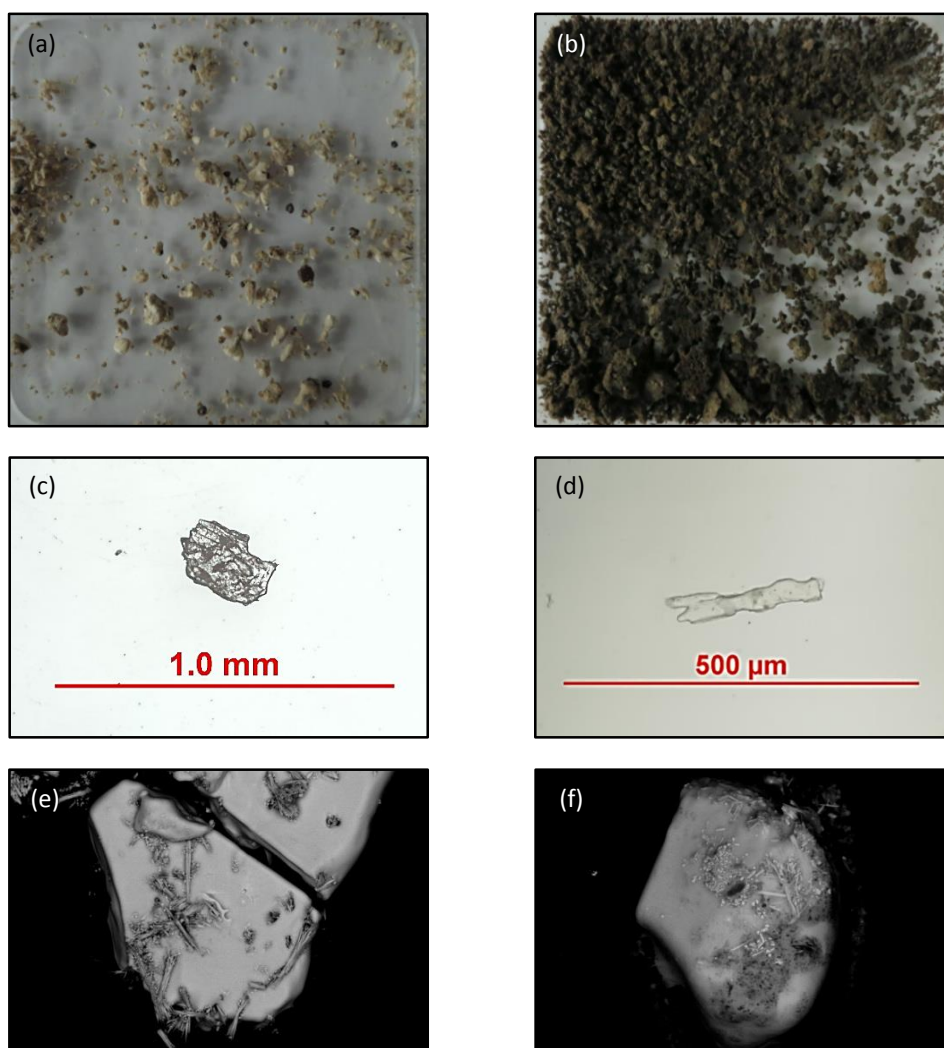


Figure 9. The sample-material with α -($C_6H_{11}N_2$) $_2$ [CdBr $_4$] (a) and β -($C_6H_{11}N_2$) $_2$ [CdBr $_4$] (b) and images of α -($C_6H_{11}N_2$) $_2$ [CdBr $_4$] (c, e) and β -($C_6H_{11}N_2$) $_2$ [CdBr $_4$] (d, f). (c) and (d) are light microscope images and (e) and (f) are BSE images.

Results

4.2.1 α -(C₆H₁₁N₂)₂[CdBr₄]

α -(C₆H₁₁N₂)₂[CdBr₄] crystallised in the space group *P*2₁/*c* and is isostructural with the compound [C₆H₁₁N₂][AuCl₄] described by Hasan et al. (1999). In the asymmetric unit of the monoclinic structure there are one crystallographically distinct cadmium atom, four crystallographically unique bromine atoms and two [emim] cations. The inorganic part of the structure consists of negatively charged [CdBr₄]²⁻ anions. Besides electrostatic forces of attraction between ions, they are crosslinked with weak hydrogen bonds to the organic part represented by positively charged [C₆H₁₁N₂]⁺ cations (Figure 10a).

The two crystallographically independent imidazolium ring systems are very similar. Each pentagon has two pairs of C–N bonds. C2–N1 [=1.319(4) Å and C2A–N1A=1.317(4) Å] and C2–N3 [=1.308(4) Å and C2A–N3A=1.318(4) Å] are shorter than the other two pairs C4–N3 [=1.374(4) Å and C4A–N3A=1.370(5) Å] and C5–N1 [=1.354(4) Å and C5A–N1A=1.365(4) Å]. The methyl groups C8H₃ and C8AH₃ are coplanar to their respective imidazolium ring, but the ethyl groups C6C7H₃ and C6AC7AH₃ are located in a way that the carbon atoms C7 and C7A, respectively, are out of plane of the imidazolium ring (Figure 10c).

Cadmium is tetrahedrally coordinated by four Br atoms. The Cd–Br bond distances are in the range from 2.5671(7) Å to 2.6228(7) Å and the Br–Cd–Br angles vary between 106.621(15)° to 112.08(3)° (Table 8 and 9). The Cd–Br bond distances and the Br–Cd–Br angles are in the range of an average [CdBr₄]²⁻ tetrahedra which ranges from 2.54 Å to 2.60 Å and 106.0° to 113.5°, respectively, according to Sharma et al. (2006).

The structure is stabilised by hydrogen bonds. [Emim] cations exhibit C–H⋯Br interactions with all of the bromine atoms (Figure 10b). The two hydrogen atoms H2 and H4A from the imidazolium rings participate in C–H⋯Br interactions. Their values range between 2.93 Å and 3.03 Å. Another five hydrogen atoms of the methyl and the ethyl groups exhibit C–H⋯Br interactions. Their values are between 2.93 Å and 3.13 Å (Table 8). Due to the long D⋯A distances (> 3.5 Å) all C–H⋯Br interactions are weak.

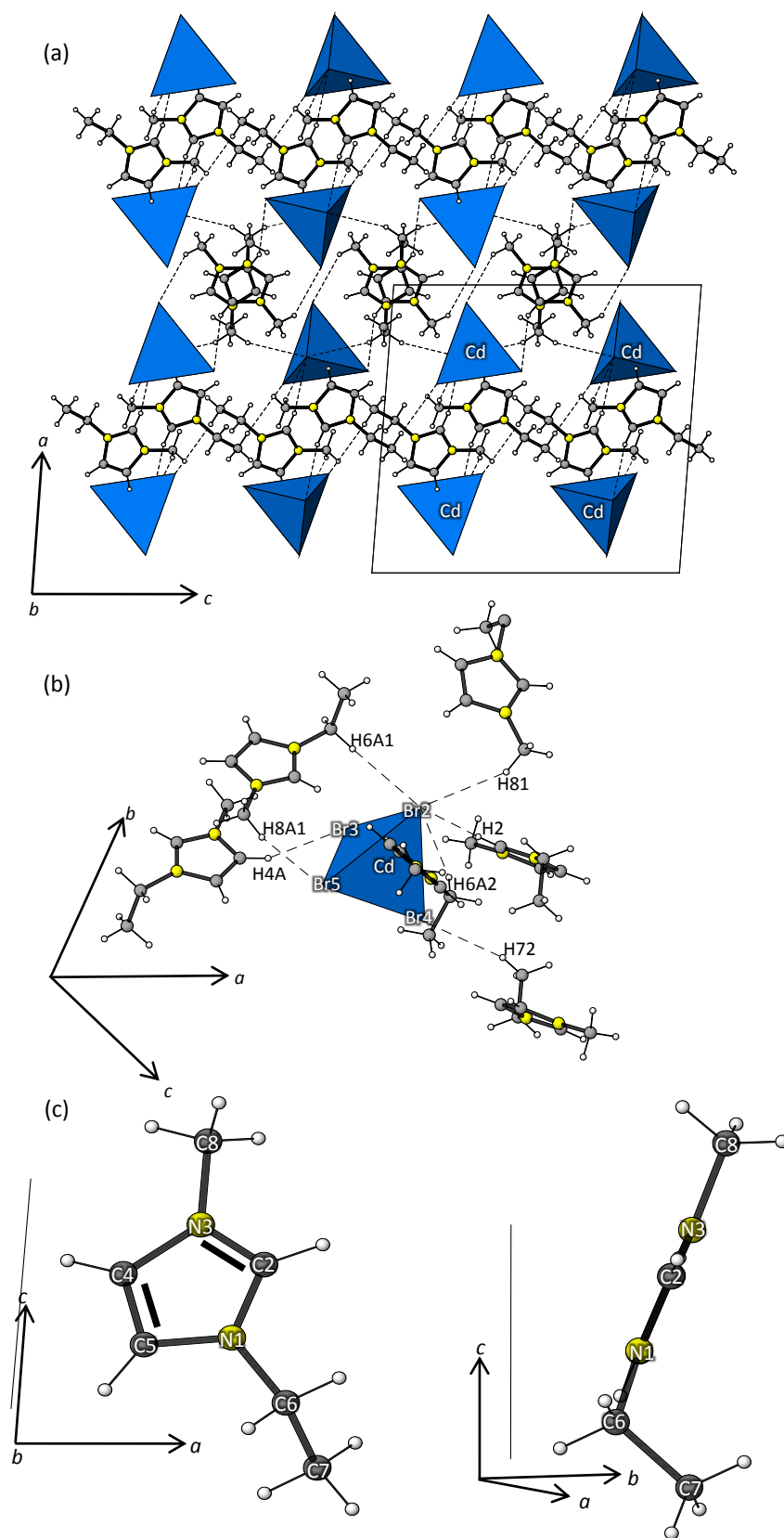


Figure 10. An overview of the structure of α -($\text{C}_6\text{H}_{11}\text{N}_2$) $_2$ [CdBr_4] (a), the hydrogen bonds (b) and the [emim] cation in detail with different perspectives of α -($\text{C}_6\text{H}_{11}\text{N}_2$) $_2$ [CdBr_4] (c).

Results

Table 6. Fractional atomic coordinates and displacement parameters for α -(C₆H₁₁N₂)₂[CdBr₄]. U_{equiv} according to Fischer and Tillmanns, (1988). For the H atoms U_{iso} is shown.

Site	x	y	z	U_{eq} / U_{iso}
Cd1	0.23875(2)	0.47631(3)	0.26937(2)	0.05041(9)
Br1	0.25011(3)	0.22852(4)	0.23426(2)	0.06184(12)
Br2	0.30007(3)	0.50571(4)	0.43659(2)	0.06496(12)
Br3	0.34484(3)	0.59973(4)	0.16403(3)	0.07161(14)
Br4	0.06156(3)	0.54004(5)	0.24045(3)	0.07877(15)
N1	0.5317(2)	0.2977(3)	0.10789(19)	0.0524(7)
C2	0.5050(3)	0.3333(3)	0.1873(3)	0.0544(9)
H2	0.4457	0.3157	0.2089	0.065
N3	0.5747(2)	0.3971(3)	0.23096(18)	0.0531(7)
C4	0.6504(3)	0.4028(4)	0.1774(3)	0.0599(10)
H4	0.7095	0.4419	0.1915	0.072
C5	0.6223(3)	0.3409(4)	0.1006(2)	0.0590(10)
H5	0.6585	0.3298	0.0513	0.071
C6	0.4703(3)	0.2327(4)	0.0371(2)	0.0702(11)
H61	0.4172	0.1910	0.0640	0.084
H62	0.5071	0.1663	0.0093	0.084
C7	0.4319(3)	0.3253(4)	-0.0330(2)	0.0707(12)
H71	0.3920	0.2799	-0.0779	0.106
H72	0.3947	0.3905	-0.0058	0.106
H73	0.4843	0.3654	-0.0607	0.106
C8	0.5739(3)	0.4499(4)	0.3219(2)	0.0823(13)
H82	0.5999	0.5358	0.3231	0.123
H81	0.6122	0.3961	0.3631	0.123
H83	0.5092	0.4523	0.3394	0.123
N1A	0.0725(2)	0.2555(3)	-0.0190(2)	0.0583(8)
C2A	0.0225(3)	0.2173(4)	-0.0927(2)	0.0592(10)
H2A	0.0409	0.2273	-0.1510	0.071
N3A	-0.0577(2)	0.1627(3)	-0.0707(2)	0.0619(8)
C4A	-0.0579(3)	0.1649(4)	0.0212(3)	0.0784(13)
H4A	-0.1055	0.1321	0.0551	0.094
C5A	0.0222(3)	0.2226(5)	0.0527(3)	0.0799(13)
H5A	0.0410	0.2379	0.1130	0.096
C6A	0.1632(3)	0.3276(4)	-0.0162(3)	0.0737(12)
H6A1	0.1996	0.3002	-0.0659	0.088
H6A2	0.2010	0.3083	0.0395	0.088
C7A	0.1458(3)	0.4699(5)	-0.0225(3)	0.0999(16)
H7A1	0.2060	0.5148	-0.0168	0.150
H7A2	0.1072	0.4965	-0.0249	0.150
H7A3	0.1128	0.4900	0.0797	0.150
C8A	-0.1339(3)	0.1120(5)	-0.1333(3)	0.0927(14)
H8A1	-0.1697	0.0479	-0.1034	0.139
H8A2	-0.1062	0.0735	-0.1839	0.139
H8A3	-0.1759	0.1811	-0.1536	0.139

Results

Table 7. Anisotropic displacement parameters for α -(C₆H₁₁N₂)₂[CdBr₄] defined as $\exp[-2\pi^2 \sum_{i=1}^3 \sum_{j=1}^3 U_{ij} a_i^* a_j^* h_i h_j]$ according to Fischer and Tillmanns (1988).

Site	U_{11}	U_{22}	U_{33}	U_{23}	U_{13}	U_{12}
Cd1	0.05065(17)	0.05165(16)	0.04916(16)	0.00137(12)	0.00518(12)	0.00291(13)
Br2	0.0737(3)	0.0486(2)	0.0623(32)	-0.00347(18)	-0.0006(2)	0.00032(19)
Br3	0.0718(3)	0.0667(3)	0.0543(2)	-0.00500(19)	-0.0086(2)	0.0078(2)
Br4	0.0805(3)	0.0653(3)	0.0719(3)	0.0054(2)	0.0248(2)	-0.0105(2)
Br5	0.0566(3)	0.1068(4)	0.0725(3)	0.0152(2)	0.0022(2)	0.0212(2)
N1	0.058(2)	0.0422(17)	0.055(2)	-0.0010(14)	-0.0036(16)	-0.0016(15)
C2	0.048(2)	0.048(2)	0.068(3)	-0.0033(19)	0.004(2)	0.0033(18)
N3	0.063(2)	0.0468(18)	0.0488(18)	-0.0041(15)	0.0033(16)	0.0003(16)
C4	0.056(2)	0.058(2)	0.065(3)	0.004(2)	-0.002(2)	-0.013(2)
C5	0.069(3)	0.060(3)	0.048(2)	-0.0005(19)	0.009(2)	-0.004(2)
C6	0.080(3)	0.061(3)	0.065(3)	-0.005(2)	-0.023(2)	-0.011(2)
C7	0.061(3)	0.084(3)	0.065(3)	0.006(2)	-0.008(2)	-0.014(2)
C8	0.110(4)	0.075(3)	0.063(3)	-0.019(2)	0.014(2)	-0.008(3)
N1A	0.051(2)	0.069(2)	0.055(2)	0.0091(16)	0.0064(17)	-0.0039(16)
C2A	0.056(3)	0.072(3)	0.050(3)	0.004(2)	0.001(2)	0.005(2)
N3A	0.059(2)	0.062(2)	0.064(2)	0.0024(17)	0.0020(18)	-0.0043(17)
C4A	0.074(3)	0.093(3)	0.070(3)	0.009(2)	0.016(2)	-0.020(3)
C5A	0.076(3)	0.113(4)	0.051(3)	0.011(2)	0.011(2)	-0.015(3)
C6A	0.057(3)	0.099(4)	0.065(3)	0.006(2)	0.001(2)	-0.006(3)
C7A	0.075(3)	0.104(4)	0.119(4)	-0.002(3)	0.000(3)	-0.034(3)
C8A	0.072(3)	0.102(4)	0.101(4)	-0.010(3)	-0.012(3)	-0.012(3)

Table 8. Selected bond distances (Å) for α -(C₆H₁₁N₂)₂[CdBr₄].

Cd1–Br5	2.5671(7)	C2–N1	1.319(4)	C2A–N1A	1.317(4)
Cd1–Br4	2.5772(7)	C2–N3	1.308(4)	C2A–N3A	1.318(4)
Cd1–Br3	2.5898(8)	C4–N3	1.374(4)	C4A–N3A	1.370(5)
Cd1–Br2	2.6228(7)	C5–N1	1.354(4)	C5A–N1A	1.365(4)
<Cd1–Br>	2.589	C4–C5	1.343(5)	C4A–C5A	1.323(5)
		C6–N1	1.471(4)	N1A–C6A	1.468(5)
		C8–N3	1.462(4)	N3A–C8A	1.458(5)
		C6–C7	1.488(5)	C6A–C7A	1.494(6)
Hydrogen bonds					
D–H···A	D–H (Å)	H···A (Å)	D···A (Å)	D–H···A (°)	
C2–H2···Br2	0.93	2.93	3.838(4)	166	
C8–H81···Br2 ⁱ	0.96	3.06	3.920(4)	150	
C7–H72···Br4 ^{iv}	0.96	2.96	3.881(4)	161	
C4A–H4A···Br3 ⁱⁱ	0.93	3.03	3.858(5)	150	
C8A–H8A1···Br5 ⁱⁱⁱ	0.96	2.92	3.775(5)	148	
C6A–H6A1···Br2 ⁱⁱⁱ	0.97	3.13	4.038(4)	157	
C6A–H6A2···Br2	0.97	3.04	3.970(4)	160	

Symmetry codes: (i) $-x+1, y+1/2, -z+1/2$; (ii) $-x, y-1/2, -z+1/2$; (iii) $x, -y+1/2, z-1/2$; (iv) $-x+1, -y+1, -z$.

Results

Table 9. Selected bond angles (°) for α -(C₆H₁₁N₂)₂[CdBr₄].

Br5–Cd1–Br4	111.27(2)		
Br5–Cd1–Br3	112.08(3)		
Br4–Cd1–Br3	111.32(2)		
Br5–Cd1–Br2	106.835(19)		
Br4–Cd1–Br2	108.44(2)		
Br3–Cd1–Br2	106.621(15)		
<Br–Cd1–Br>	109.4277		
C2–N1–C5	108.0(3)	C2A–N1A–C5A	107.8(3)
C2–N1–C6	125.5(3)	C2A–N1A–C6A	125.3(3)
C5–N1–C6	126.3(3)	C5A–N1A–C6A	126.9(3)
N3–C2–N1	109.6(3)	N3A–C2A–N1A	109.2(3)
C2–N3–C4	108.0(3)	C2A–N3A–C4A	107.9(3)
C2–N3–C8	126.3(3)	C2A–N3A–C8A	126.1(4)
C4–N3–C8	125.6(3)	C4A–N3A–C8A	126.0(4)
C5–C4–N3	106.6(3)	C5A–C4A–N3A	107.2(4)
C4–C5–N1	107.7(3)	C4A–C5A–N1A	107.9(4)
N1–C6–C7	111.6(3)	N1A–C6A–C7A	111.2(3)

4.2.2 β -(C₆H₁₁N₂)₂[CdBr₄]

The tetragonal variant of the inorganic-organic hybrid crystallises in the space group $I4_1/a$ and is isostructural with [emim]₂[CoCl₄] and [emim]₂[NiCl₄] described by Hitchcock et al. (1993). In the asymmetric unit of the structure there are two crystallographically distinct cadmium atoms and two crystallographically unique bromine atoms and one [emim] cation. The inorganic part of the structure is represented by the two [CdBr₄]²⁻-tetrahedra and the organic part is by [emim] cation. Like in the monoclinic polymorph, they are crosslinked with hydrogen bonds (Figure 11a).

Similar to the monoclinic polymorph, the tetragonal structure has planar imidazolium pentagons as well as the monoclinic structure, but the ethyl and methyl groups are planar to the rings (Figure 11c) which also leads to different bond lengths. The C–N length of C4–N3 [=1.332(11) Å] is shorter than the C2–N3 bond length [1.375(12) Å], which is unusual for the [emim] cation.

The two unique Cd atoms occupy special positions with a quarter-occupancy. They are located at a four-fold rotoinversion axis parallel to the *c*-axis (site symmetry $\bar{4}$). As a result, both cadmium tetrahedra have a crystallographically imposed $\bar{4}$ symmetry. The distance of Cd1–Br4 with 2.5769(8) Å is slightly shorter than the bond distance of Cd2–Br3 with 2.5788(8) Å. The bond angles of [Cd1Br₄]²⁻ equal 110.00(2)°, 108.43(5)° and 109.99(2)° and the bond angles of the slightly more distorted [Cd2Br₃]²⁻ equal 107.78(2)° and 112.90(4)° (Table 12 and 13). These values are in the range of an average [CdBr₄]²⁻ tetrahedra according to Sharma et al. (2006).

The 3D network of the structure can be established *via* the C–H⋯Br interactions involving the hydrogen atoms H2, H4 and H5 of the imidazolium ring (Figure 11b). The hydrogen atoms of the methyl and ethyl groups are not involved. All hydrogen connections are weak because all D⋯A distances are longer than 3.5 Å (Table 12).

Results

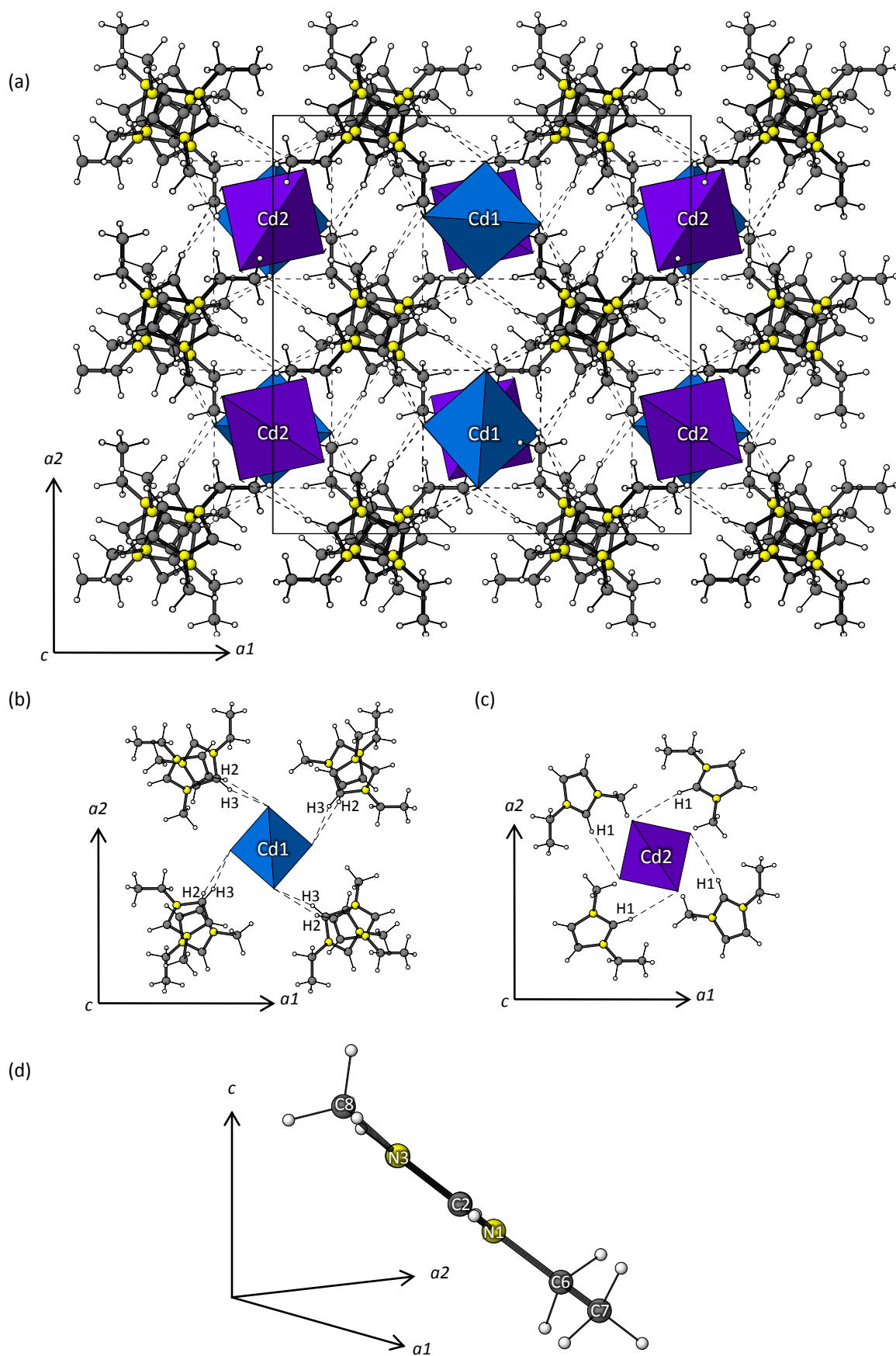


Figure 11. An overview of the structure of $\beta\text{-}(\text{C}_6\text{H}_{11}\text{N}_2)_2[\text{CdBr}_4]$ (a), the hydrogen bonds (b, c) and the [emim] cation of $\beta\text{-}(\text{C}_6\text{H}_{11}\text{N}_2)_2[\text{CdBr}_4]$ (d).

Results

Table 10. Fractional atomic coordinates and displacement parameters for β -(C₆H₁₁N₂)₂[CdBr₄]. U_{equiv} according to Fischer and Tillmanns, (1988). For the H atoms U_{iso} is shown.

Site	x	y	z	U_{eq} / U_{iso}
Cd1	0.0000	0.2500	0.1250	0.0538(3)
Cd2	0.0000	0.7500	0.3750	0.0540(3)
Br3	0.00933(6)	0.39032(6)	0.05186(5)	0.0970(3)
Br4	0.12140(6)	0.67144(5)	0.30581(4)	0.0833(3)
N1	0.1972(6)	0.5733(6)	0.1540(4)	0.100(2)
C2	0.2637(7)	0.6062(7)	0.1843(5)	0.096(3)
H2	0.2826	0.6658	0.1829	0.115
N3	0.3031(6)	0.5383(6)	0.2197(4)	0.109(3)
C4	0.2563(8)	0.4636(7)	0.2080(5)	0.112(3)
H4	0.2681	0.4067	0.2248	0.134
C5	0.1863(7)	0.4863(7)	0.1659(5)	0.106(3)
H5	0.1417	0.4486	0.1497	0.128
C6	0.1397(12)	0.6242(10)	0.1134(6)	0.165(6)
H61	0.1414	0.5931	0.0720	0.199
H62	0.0800	0.6137	0.1308	0.199
C7	0.1403(17)	0.7056(13)	0.0989(11)	0.315(15)
H71	0.0907	0.7183	0.0704	0.472
H72	0.1957	0.7201	0.0774	0.472
H73	0.1347	0.7411	0.1376	0.472
C8	0.3833(8)	0.5497(10)	0.2673(7)	0.190(7)
H82	0.4039	0.6109	0.2661	0.285
H81	0.4314	0.5103	0.2547	0.285
H83	0.3641	0.5351	0.3105	0.285

Table 11. Anisotropic displacement parameters defined for β -(C₆H₁₁N₂)₂[CdBr₄] as $\exp[-2\pi^2 \sum_{i=1}^3 \sum_{j=1}^3 U_{ij} a_i^* a_j^* h_i h_j]$ according to Fischer and Tillmanns (1988).

Site	U_{11}	U_{22}	U_{33}	U_{23}	U_{13}	U_{12}
Cd1	0.0502(3)	0.0502(3)	0.0610(6)	0.000	0.000	0.000
Cd2	0.0568(4)	0.0568(4)	0.0484(5)	0.000	0.000	0.000
Br3	0.0760(6)	0.0992(6)	0.1159(7)	0.0556(5)	-0.0123(5)	-0.0131(4)
Br4	0.0953(6)	0.0685(5)	0.0860(5)	-0.0158(4)	0.0402(4)	-0.0061(4)
N1	0.105(6)	0.098(6)	0.097(6)	-0.023(5)	0.028(5)	-0.011(5)
C2	0.097(7)	0.081(6)	0.110(7)	-0.017(6)	0.046(6)	-0.028(6)
N3	0.114(7)	0.085(6)	0.128(7)	-0.014(5)	0.044(5)	-0.022(5)
C4	0.129(9)	0.079(6)	0.128(9)	-0.002(6)	0.029(7)	-0.014(6)
C5	0.117(8)	0.072(6)	0.129(9)	-0.024(6)	0.014(7)	-0.025(6)
C6	0.238(17)	0.128(11)	0.130(10)	0.017(9)	-0.018(10)	0.047(12)
C7	0.38(3)	0.20(2)	0.36(3)	-0.22(3)	-0.22(3)	0.01(2)
C8	0.100(9)	0.223(16)	0.247(16)	0.107(13)	-0.031(10)	-0.050(10)

Results

Table 12. Selected bond distances (Å) for β -(C₆H₁₁N₂)₂[CdBr₄].

Cd1–Br3 ⁱ	2.5767(8)	Cd2–Br4 ^{iv}	2.5789(8)	C2–N1	1.268(11)
Cd1–Br3 ⁱⁱ	2.5767(8)	Cd2–Br4 ^v	2.5789(8)	C2–N3	1.375(12)
Cd1–Br3 ⁱⁱⁱ	2.5767(8)	Cd2–Br4 ^{vi}	2.5789(8)	C4–N3	1.332(11)
Cd1–Br3	2.5767(8)	Cd2–Br4	2.5789(8)	C5–N1	1.326(11)
<Cd1–Br>	2.5767	<Cd2–Br>	2.5789	N1–C6	1.414(14)
				N3–C8	1.554(14)
				C4–C5	1.395(13)
				C6–C7	1.25(2)

Symmetry codes: (i) $-x, -y+1/2, z$; (ii) $y-1/4, -x+1/4, -z+1/4$; (iii) $-y+1/4, x+1/4, -z+1/4$; (iv) $-y+3/4, x+3/4, -z+3/4$; (v) $-x, -y+3/2, z$; (vi) $y-3/4, -x+3/4, -z+3/4$;

Hydrogen bonds				
D–H⋯A	D–H (Å)	H⋯A (Å)	D⋯A (Å)	D–H⋯A (°)
C2–H2⋯Br3 ^{viii}	0.93	2.82	3.726(9)	166
C4–H4⋯Br4 ^{vii}	0.93	3.03	3.914(12)	160
C5–H5⋯Br4	0.93	2.95	3.805(11)	154

Symmetry codes: (vii) $-y+3/4, x+1/4, z+1/4$; (viii) $-x+1/2, -y+3/2, -z+1/2$;

Table 13. Selected bond angles (°) for β -(C₆H₁₁N₂)₂[CdBr₄].

Br4 ⁱ –Cd1–Br4 ⁱⁱ	109.99(3)	C2–N1–C5	112.3(10)
Br4 ⁱ –Cd1–Br4 ⁱⁱⁱ	109.99(3)	C2–N1–C6	123.8(11)
Br4 ⁱⁱ –Cd1–Br4 ⁱⁱⁱ	108.43(5)	C5–N1–C6	123.9(11)
Br4 ⁱ –Cd1–Br4	108.43(5)		
Br4 ⁱⁱ –Cd1–Br4	109.99(3)	N3–C2–N1	108.1(9)
Br4 ⁱⁱⁱ –Cd1–Br4	110.00(3)		
<Br4–Cd1–Br4>	109.46	C2–N3–C4	107.1(9)
		C2–N3–C8	125.5(9)
Br3 ^{iv} –Cd2–Br3 ^v	107.79(2)	C4–N3–C8	127.3(11)
Br3 ^{vi} –Cd2–Br3 ^{vi}	112.90(4)		
Br3 ^v –Cd2–Br3 ^{vi}	107.79(2)	N3–C4–C5	107.4(9)
Br3 ^{iv} –Cd2–Br3	107.79(2)	C4–C5–N1	105.1(9)
Br3 ^v –Cd2–Br3	112.90(4)	N1–C6–C7	131.1(17)
Br3 ^{vi} –Cd2–Br3	107.78(2)		
<Br3–Cd2–Br3>	109.49		

Symmetry codes: (i) $-x, -y+1/2, z$; (ii) $y-1/4, -x+1/4, -z+1/4$; (iii) $-y+1/4, x+1/4, -z+1/4$; (iv) $-y+3/4, x+3/4, -z+3/4$; (v) $-x, -y+3/2, z$; (vi) $y-3/4, -x+3/4, -z+3/4$;

4.2.3 Infrared spectra of α - and β -(C₆H₁₁N₂)₂[CdBr₄]

Both spectra (Figure 12) show two peaks above 3000 cm⁻¹, at 3137 cm⁻¹ and 3114 cm⁻¹ for the monoclinic crystal and 3134 cm⁻¹ and 3101 cm⁻¹ for the tetragonal crystal, which can be attributed to aromatic C–H stretching (Tait and Osteryoung, 1984). These peaks represent the stretching vibrations of [C4–H], [C5–H] and [C2–H] and they are highly characteristic for imidazolium rings (Rogalski et al., 2013). Their relatively low values confirm the presence of weak hydrogen bonds to the [CdBr₄]²⁻ tetrahedra. A higher wave number would testify for a diminution or absence of hydrogen-bonds (Larsen et al., 2000).

Peaks below 3000 cm⁻¹, at 2970 cm⁻¹ for α -(C₆H₁₁N₂)₂[CdBr₄] and 2985 cm⁻¹ for β -(C₆H₁₁N₂)₂[CdBr₄], can be attributed to aliphatic C–H stretching (Tait and Osteryoung, 1984). The aliphatic C–H bending vibrations [δ (CH₂), δ (CH₃), δ_{as} (CH₃)] are located between 1470 cm⁻¹ and 1380 cm⁻¹ (Katsyuba et al., 2004) and represented by the peak at 1444 cm⁻¹ for the monoclinic crystal and at 1460 cm⁻¹ for the tetragonal crystal.

Other vibrations caused by the [emim]-ring are located at 1585 cm⁻¹ and 1568 cm⁻¹ for the monoclinic crystal and at 1578 cm⁻¹ for the tetragonal crystal. They show the stretching vibrations of C=C and the stretching vibrations of C–N. Peaks located at 1337 cm⁻¹ and 1172 cm⁻¹ for α -(C₆H₁₁N₂)₂[CdBr₄] and 1342 cm⁻¹ and 1162 cm⁻¹ for β -(C₆H₁₁N₂)₂[CdBr₄] represent the stretching vibrations between the alkyl chains and N (Katsyuba et al., 2004).

All peaks below 850 cm⁻¹ represent out of plane vibrations of the [emim] cation (Katsyuba et al., 2004). The most intense peaks are located at 842 cm⁻¹, 732 cm⁻¹ and 646 cm⁻¹ for the monoclinic crystal and at 854 cm⁻¹, 775 cm⁻¹ and 621 cm⁻¹ for the tetragonal crystal.

Even if there is no water in the structures of the hybrids, O–H vibrations may still be present because of the strong hygroscopic character of the ionic liquid [emim]Br.

Results

Table 14. The most intense peaks of the spectra of α - and β -($C_6H_{11}N_2$) $_2$ [$CdBr_4$].

type of vibration	$\bar{\nu}$ [cm^{-1}] monoclinic	$\bar{\nu}$ [cm^{-1}] tetragonal
aromatic C–H stretching vibrations	3137, 3114	3134, 3101
aliphatic C–H stretching vibrations	2970	2985
$\nu(C=C)$, $\nu(C-N)$	1585, 1568	1578
aliphatic C–H bending vibrations	1444	1460
ν (Ethyl–N), ν (Methyl–N)	1337, 1172	1342, 1162
out of plane vibrations of the [emim] cation	842, 732, 646	854, 775, 621

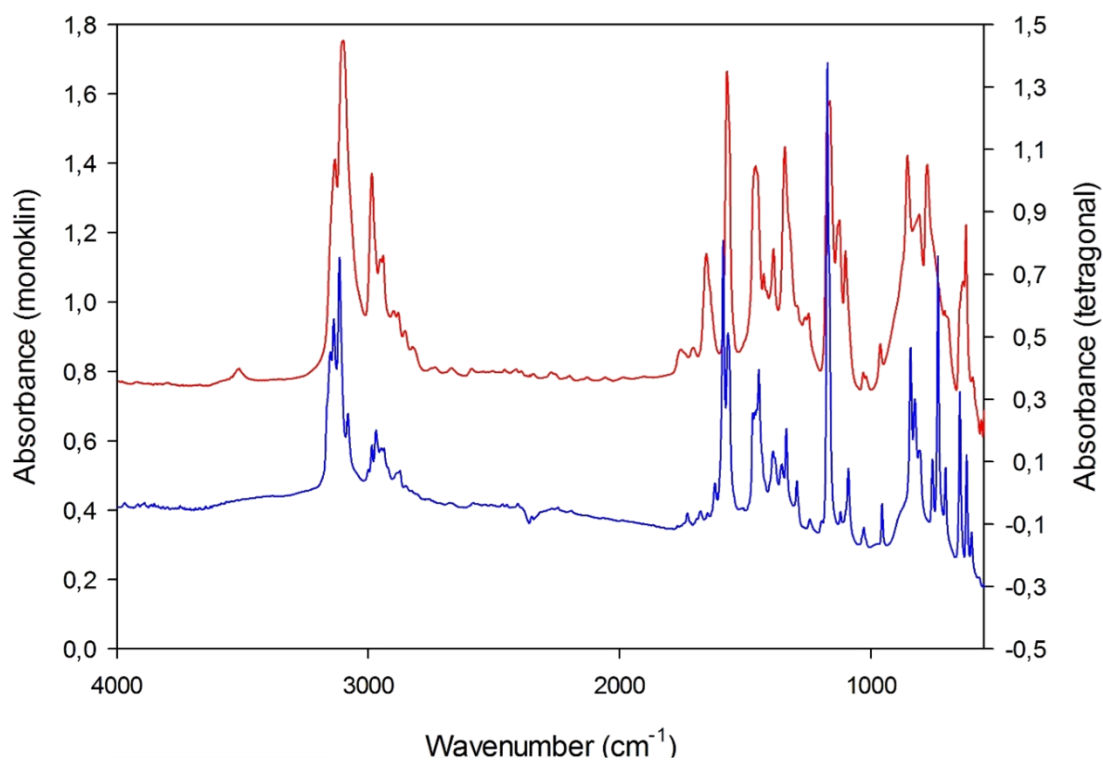


Figure 12. IR-spectra of α -($C_6H_{11}N_2$) $_2$ [$CdBr_4$] (blue) and β -($C_6H_{11}N_2$) $_2$ [$CdBr_4$] (red).

4.3 $\text{Zn}_9(\text{AsO}_4)_6(\text{H}_2\text{O})_4$

At 160°C a cadmium free zinc-arsenate was obtained together with $\alpha\text{-(C}_6\text{H}_{11}\text{N}_2)_2[\text{CdBr}_4]$. The crystals of $\text{Zn}_9(\text{AsO}_4)_6(\text{H}_2\text{O})_4$ are colourless, with a maximum size of 0.4 mm, have a prismatic shape and are often grown together. The SEM-EDS analysis of the crystal confirms the presence of Zn, As and O (Table 5).

It is a known crystal structure, first published by Feng et al. (1997), but synthesised for the first time by using an ionic liquid as solvent. The structure has been re-refined starting from the atomic coordinates of $\text{Zn}_9(\text{AsO}_4)_6 \cdot 4(\text{H}_2\text{O})$ (Jensen et al. 1998). All hydrogen atoms were detected in the electron density map and their positions were isotropically refined.

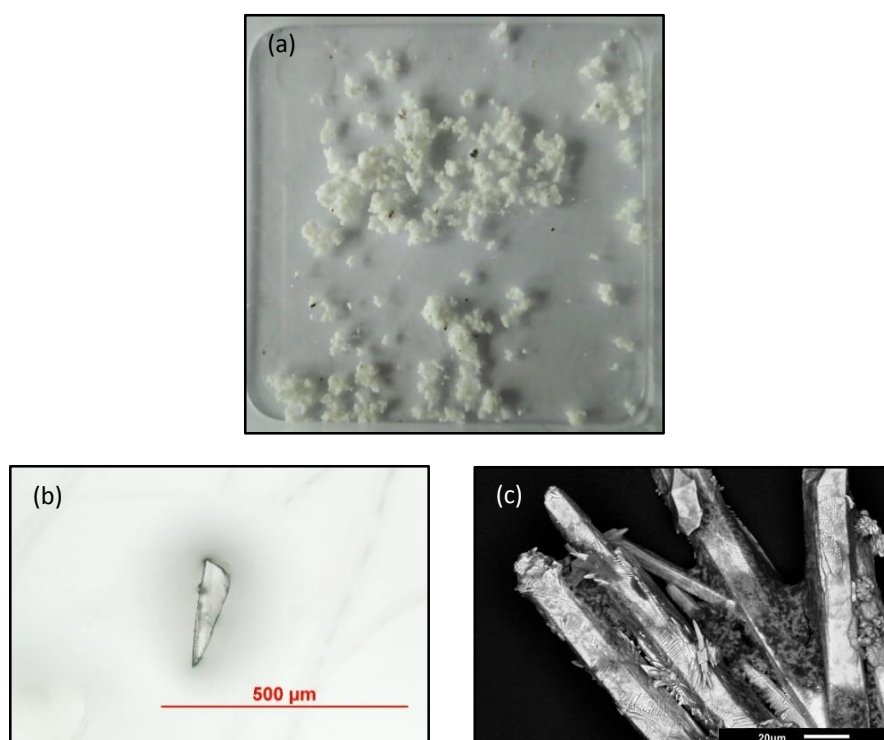


Figure 13. The sample material with $\text{Zn}_9(\text{AsO}_4)_6(\text{H}_2\text{O})_4$ (a) and the single crystal (b, c). (b) is a light microscope image and (c) is a BSE image of $\text{Zn}_9(\text{AsO}_4)_6(\text{H}_2\text{O})_4$.

4.3.1 Structure description

The crystal structure of $\text{Zn}_9(\text{AsO}_4)_6(\text{H}_2\text{O})_4$ has three distinct arsenic tetrahedra and five unique zinc positions which appear in three different coordinations. Zn1, Zn2 and Zn4 are octahedrally coordinated. Zn2 is tetrahedrally coordinated and Zn5 adopts a trigonal bipyramidal coordination.

The framework of the structure is built up of an infinite chain of $\text{Zn}(\text{O},\text{OH})_x$ ($x = 4-6$), polyhedral in the sequence $\text{Zn}_5\text{O}_5-\text{Zn}_3\text{O}_6-\text{Zn}_1\text{O}_4(\text{OH}_2)_2-\text{Zn}_3\text{O}_6-\text{Zn}_4\text{O}_5(\text{OH}_2)-\text{Zn}_4\text{O}_5(\text{OH}_2)$ and a cluster of eight corner sharing tetrahedra (Figure 14). The three Zn octahedra and the trigonal bipyramidal coordinated Zn5, which are interconnected *via* edges, build up an infinite zigzag chain along the crystallographic [111] direction. Due to the location of Zn1 on the special position $(0, 0, \frac{1}{2})$ the $\text{Zn}_1\text{O}_4(\text{OH}_2)_2$ octahedra is centrosymmetric and the chain of Zn polyhedra has an inversion symmetry. Furthermore, the cluster of tetrahedra is located at the centre of inversion. All three As tetrahedra and the Zn_2O_4 tetrahedra are involved in the cluster. The chains are interconnected *via* the cluster and hydrogen bonds, forming a 3D network (Figure 14a).

The As–O distances in $\text{Zn}_9(\text{AsO}_4)_6(\text{H}_2\text{O})_4$ vary from 1.6590(19) Å to 1.7211(19) Å. Furthermore, the Zn–O distances of the three Zn octahedra range from 2.068(2) Å to 2.225(2) Å for the $\text{Zn}_1\text{O}_4(\text{OH}_2)_2$ octahedra, from 1.987(2) Å to 2.476(2) Å for the Zn_3O_6 octahedra and from 2.0754(19) Å to 2.117(2) Å for the $\text{Zn}_4\text{O}_5(\text{OH}_2)$ octahedra. The Zn–O distances for the trigonal bipyramidal polyhedra and the Zn_2O_4 tetrahedra vary from 1.930(2) Å to 2.2409(19) Å and from 1.891(2) Å to 1.9773(19) Å, respectively (Table 17).

Four different hydrogen bonds are present in the structure involving the two water molecules ($\text{H}_2\text{OW1}$, $\text{H}_2\text{OW2}$) which are situated in the channels along the [101] direction (Figure 14a). The water molecule $\text{H}_2\text{OW1}$ is located at the corners of the Zn1 octahedra and Zn3 octahedra while the second water molecule, $\text{H}_2\text{OW2}$, is only coordinated to Zn4. The two water molecules build up four different hydrogen bonds with O3 and O9 as acceptors for the hydrogen bond donor OW1 and O6 and O11 as acceptors for the hydrogen bond donor OW2. The D...A distances are in the range from 2.641(3) Å to 3.006(3) Å. Hence, the bonds can be considered as intermediately strong to weak hydrogen bonds. The bond valence calculation

Results

also confirms the location of the hydrogen bonds. All oxygen atoms which are included in hydrogen bonding are undersaturated (for detailed values Table 19). The values for the other oxygen atoms are close to the nominal valence of 2+.

The degree of distortion of the tetrahedra and octahedra was calculated using the three distortion indices (DI) by Baur (1974) (Equation 1). TO stands for distances from the cation to the oxygen atom, OTO for the angles O–T–O, OO for the lengths of the polyhedron edges, m signifies the mean value for the polyhedra and i the individual value for the polyhedron (Table 19).

Equation 1. The three equations for the distortion indices for tetrahedra and octahedra, respectively.

$$\begin{aligned}
 \text{DI}(\text{TO})_{tet} &= (\Sigma|\text{TO}_i - \text{TO}_m|)/4\text{TO}_m & \text{DI}(\text{TO})_{oct} &= (\Sigma|\text{TO}_i - \text{TO}_m|)/6\text{TO}_m \\
 \text{DI}(\text{OTO})_{tet} &= (\Sigma|\text{OTO}_i - \text{OTO}_m|)/6\text{OTO}_m & \text{DI}(\text{OTO})_{oct} &= (\Sigma|\text{OTO}_i - \text{OTO}_m|)/12\text{OTO}_m \\
 \text{DI}(\text{OO})_{tet} &= (\Sigma|\text{OO}_i - \text{OO}_m|)/6\text{OO}_m & \text{DI}(\text{OO})_{oct} &= (\Sigma|\text{OO}_i - \text{OO}_m|)/12\text{OO}_m
 \end{aligned}$$

Furthermore, the disorder parameter bond angle variance (σ^2) and mean quadratic elongation (λ) introduced by Robinson et al. (1971) and Fleet (1976) (Equation 2) were determined for the As-tetrahedra and the Zn-polyhedra (Table 20).

Equation 2. The two equations for the disorder parameter of tetrahedra and octahedra, respectively.

$$\begin{aligned}
 \sigma_{tet}^2 &= \frac{1}{5} \Sigma(\angle_i - 109.47^\circ)^2 & \lambda_{tet} &= \frac{1}{4} \Sigma[(l_i - l_m)/l_m]^2 \\
 \sigma_{oct}^2 &= \frac{1}{11} \Sigma(\angle_i - 90^\circ)^2 & \lambda_{oct} &= \frac{1}{6} \Sigma[(l_i - l_m)/l_m]^2
 \end{aligned}$$

The distortion parameters testify that the As tetrahedra are not distorted at all but the Zn polyhedra show an angle distortion. The angles of the Zn1 octahedra are strongly distorted while the other four Zn polyhedra are only intermediately distorted. All calculated values agree with the distortion indices and disorder parameters calculated from the data of the structures described by Feng et al. (1997) and Jensen et al. (1998).

Results

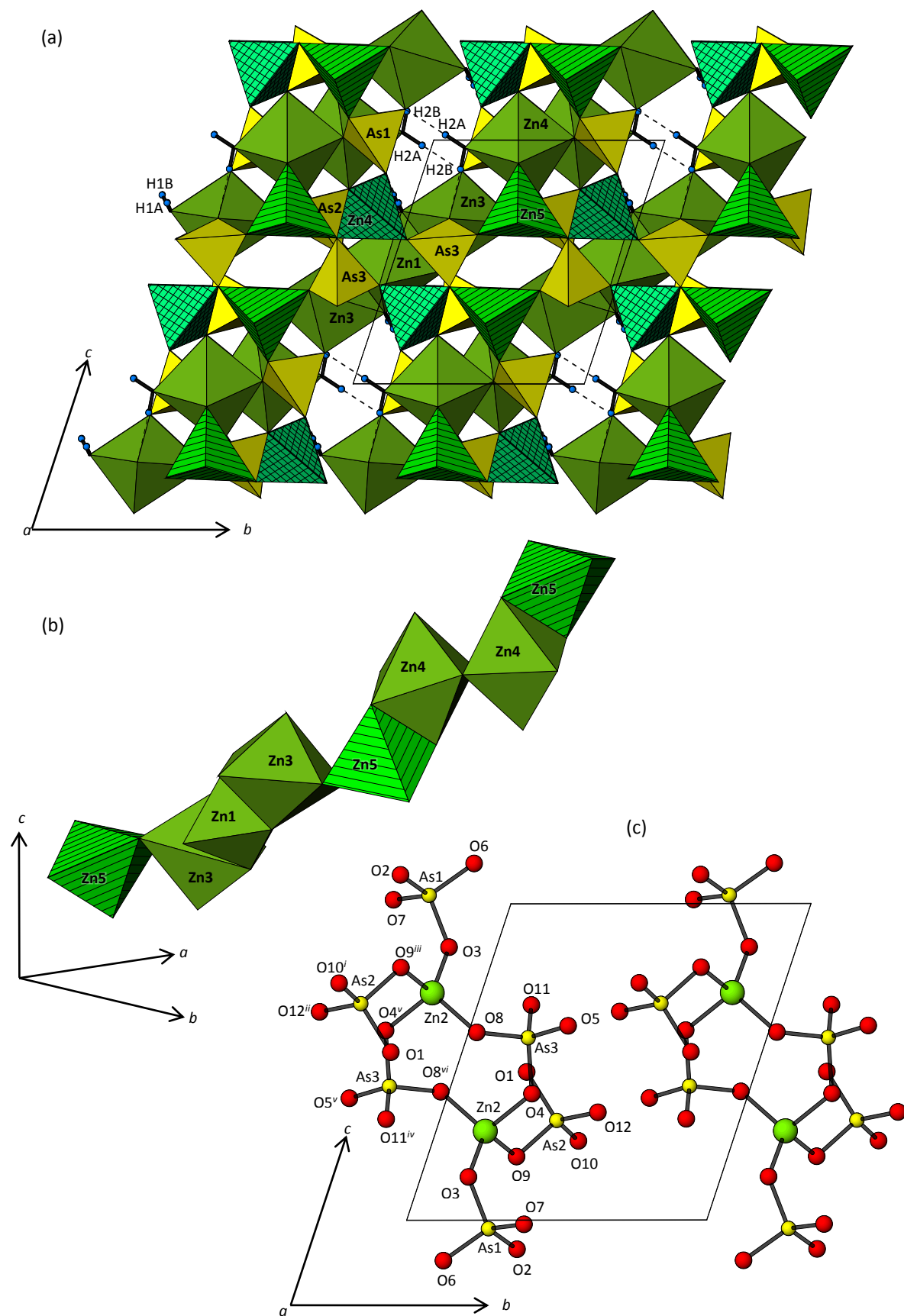


Figure 14. An illustration of the whole structure of $Zn_9(AsO_4)_6(H_2O)_4$ (a), the edge sharing Zn polyhedra chain along the [111] (b) and the cluster of As- and Zn-tetrahedra (c).

Results

Table 15. Fractional atomic coordinates and displacement parameters of $\text{Zn}_9(\text{AsO}_4)_6(\text{H}_2\text{O})_4$. U_{equiv} according to Fischer and Tillmanns, (1988). For the H atoms U_{iso} is shown.

Site	x	y	z	$U_{\text{eq}} / U_{\text{iso}}$
Zn1	0.0000	1.0000	0.5000	0.01189(9)
Zn2	0.56648(5)	0.83563(4)	-0.28120(3)	0.01121(7)
Zn3	0.03487(5)	0.74835(4)	0.33276(3)	0.01262(7)
Zn4	0.79614(5)	0.61741(4)	0.02418(3)	0.01098(7)
Zn5	0.47974(5)	0.50656(4)	0.30231(3)	0.01042(7)
As1	0.26611(4)	0.71834(3)	0.02669(3)	0.00818(6)
As2	-0.01832(4)	0.60900(3)	0.68564(3)	0.00767(6)
As3	0.49781(4)	0.79540(3)	-0.57659(3)	0.00838(6)
O1	0.0071(3)	0.7622(2)	0.53227(19)	0.0120(4)
O2	0.4844(3)	0.6004(2)	0.0918(2)	0.0115(4)
O3	0.3342(3)	0.8418(2)	-0.1370(2)	0.0140(4)
O4	0.5158(3)	0.7214(2)	-0.3999(2)	0.0117(4)
O5	0.3837(3)	0.6753(3)	0.3856(2)	0.0176(4)
O6	0.1423(3)	0.8335(2)	0.1272(2)	0.0155(4)
O7	0.1139(3)	0.6047(2)	0.0125(2)	0.0126(4)
O8	0.6651(3)	1.0272(2)	-0.4061(2)	0.0121(4)
O9	0.8184(3)	0.7032(2)	-0.2005(2)	0.0111(4)
O10	0.7966(3)	0.4860(2)	0.2493(2)	0.0123(4)
O11	-0.2757(3)	0.8205(3)	0.3202(2)	0.0149(4)
O12	0.1343(3)	0.5193(2)	0.3402(2)	0.0127(4)
OW1	-0.0277(3)	1.0369(3)	0.2912(2)	0.0148(4)
OW2	0.7220(4)	0.8542(3)	0.0304(3)	0.0225(5)
H1A	-0.141(3)	1.063(4)	0.256(3)	0.018
H1B	0.049(4)	1.097(3)	0.227(3)	0.018
H2A	0.766(5)	0.941(2)	-0.014(3)	0.027
H2B	0.735(5)	0.858(3)	0.1108(2)	0.027

Results

Table 16. Anisotropic displacement parameters for $\text{Zn}_9(\text{AsO}_4)_6(\text{H}_2\text{O})_4$ defined as $\exp[-2\pi^2 \sum_{i=1}^3 \sum_{j=1}^3 U_{ij} a_i^* a_j^* h_i h_j]$ according to Fischer and Tillmanns (1988).

Site	U_{11}	U_{22}	U_{33}	U_{23}	U_{13}	U_{12}
Zn1	0.0165(2)	0.0093(2)	0.0108(2)	-0.00374(16)	-0.00267(16)	-0.00264(16)
Zn2	0.01055(15)	0.01137(15)	0.01095(14)	-0.00295(11)	-0.00086(11)	-0.00216(11)
Zn3	0.01451(16)	0.01388(16)	0.00932(14)	-0.00544(12)	-0.00035(11)	-0.00095(12)
Zn4	0.00873(14)	0.01351(16)	0.00983(14)	-0.00319(11)	-0.00072(11)	-0.00175(11)
Zn5	0.01184(15)	0.00959(15)	0.00959(14)	-0.00327(11)	-0.00088(11)	-0.00175(11)
As1	0.00748(12)	0.00957(13)	0.00703(11)	-0.00250(9)	-0.00064(9)	-0.00128(9)
As2	0.00712(12)	0.00849(12)	0.00754(11)	-0.00265(9)	-0.00127(9)	-0.00134(9)
As3	0.00872(12)	0.00833(12)	0.00850(12)	-0.00294(9)	-0.00141(9)	-0.00174(9)
O1	0.0166(9)	0.0128(10)	0.0065(8)	-0.0025(7)	0.0000(7)	-0.0048(7)
O2	0.0092(9)	0.0147(10)	0.0103(8)	-0.0039(7)	-0.0024(7)	-0.0007(7)
O3	0.0126(9)	0.0154(10)	0.0086(8)	0.0015(7)	0.0011(7)	-0.0032(7)
O4	0.0163(9)	0.0119(9)	0.0070(8)	-0.0015(7)	-0.0028(7)	-0.0039(7)
O5	0.0139(10)	0.0228(12)	0.0254(11)	-0.0185(9)	0.0002(8)	-0.0066(8)
O6	0.0193(10)	0.0125(10)	0.0129(9)	-0.0058(8)	0.0014(8)	-0.0004(8)
O7	0.0110(9)	0.0155(10)	0.0149(9)	-0.0079(8)	-0.0026(7)	-0.0039(7)
O8	0.0099(9)	0.0080(9)	0.0158(9)	-0.0019(7)	-0.0013(7)	-0.0002(7)
O9	0.0098(9)	0.0142(10)	0.0087(8)	-0.0050(7)	-0.0014(7)	0.0009(7)
O10	0.0078(8)	0.0150(10)	0.0121(9)	-0.0019(7)	-0.0028(7)	-0.0008(7)
O11	0.0107(9)	0.0193(11)	0.0123(9)	-0.0016(8)	0.0005(7)	-0.0052(8)
O12	0.0110(9)	0.0117(9)	0.0190(10)	-0.0069(8)	-0.0036(7)	-0.0041(7)
OW1	0.0128(10)	0.0212(11)	0.0120(9)	-0.0038(8)	-0.0030(7)	-0.0068(8)
OW2	0.0276(12)	0.0197(12)	0.0246(12)	-0.0093(10)	-0.0071(10)	-0.0057(9)

Results

Table 17. Selected bond distances (Å) for Zn₉(AsO₄)₆(H₂O)₄.

As-tetrahedra					
As1–O6	1.674(2)	As2–O10 ⁱ	1.672(2)	As3–O11 ^{iv}	1.6590(19)
As1–O7	1.6869(19)	As2–O12 ⁱⁱ	1.6790(19)	As3–O5 ^v	1.670(2)
As1–O3	1.688(2)	As2–O1	1.701(2)	As3–O8 ^{vi}	1.699(2)
As1–O2	1.7013(19)	As2–O9 ⁱⁱⁱ	1.7211(19)	As3–O4	1.7003(19)
<As1–O>	1.687	<As2–O>	1.695	<As3–O>	1.682
Zn-polyhedra					
Zn1–OW1	2.068(2)	Zn3–O6	1.987(2)	Zn4–O2	2.0754(19)
Zn1–OW1 ^{vii}	2.068(2)	Zn3–O12	2.025(2)	Zn4–O7 ^{ix}	2.0820(19)
Zn1–O1	2.083(2)	Zn3–O1	2.0377(19)	Zn4–O9	2.118(2)
Zn1–O1 ^{vii}	2.083(2)	Zn3–O11	2.041(2)	Zn4–O7 ^x	2.121(2)
Zn1–O8 ⁱⁱⁱ	2.225(2)	Zn3–O5	2.393(2)	Zn4–OW2	2.130(2)
Zn1–O8 ^{viii}	2.225(2)	Zn3–OW1	2.476(2)	Zn4–O10	2.177(2)
<Zn1–O>	2.125	<Zn3–O>	2.160	<Zn4–O>	2.116
Zn2–O3	1.891(2)			Zn5–O5	1.930(2)
Zn2–O8	1.943(2)			Zn5–O4 ^x	1.973(2)
Zn2–O9	1.975(2)			Zn5–O2	1.999(2)
Zn2–O4 ^v	1.9773(19)			Zn5–O10	2.0494(19)
<Zn2–O>	1.948			Zn5–O12	2.2409(19)
				<Zn5–O>	2.038

symmetry code: (i) -x+1, -y+1, -z+1; (ii) -x, -y+1, -z+1; (iii) x-1, y, z+1; (iv) x+1, y, z-1; (v) x, y, z-1; (vi) -x+1, -y+2, -z-1; (vii) -x, -y+2, -z+1; (viii) -x+1, -y+2, -z; (ix) x+1, y, z; (x) -x+1, -y+1, -z.;

Hydrogen bonds				
D–H...A	D–H (Å)	H...A (Å)	D...A (Å)	D–H...A (°)
OW1–H1A...O3 ^{xiii}	0.86(1)	1.81(1)	2.641(3)	162(3)
OW1–H1B...O9 ^{xi}	0.86(1)	2.14(2)	2.837(3)	138(3)
OW2–H2A...O6 ^{xi}	0.86(1)	2.15(1)	3.006(3)	177(3)
OW2–H2B...O11 ^{xii}	0.86(1)	2.02(1)	2.850(3)	165(1)

symmetry code: (xi) -x+1, -y+2, -z; (xii) x+1, y, z; (xiii) -x, -y+2, -z.;

Results

Table 18. Selected bond angles (°) for Zn₉(AsO₄)₆(H₂O)₄.

As-Tetrahedra					
O7–As1–O6	112.66(10)	O12 ⁱⁱ –As2–O10 ⁱ	109.85(10)	O5 ^v –As3–O11 ^{iv}	112.14(10)
O3–As1–O6	106.25(11)	O1–As2–O10 ⁱ	115.13(10)	O8 ^{vi} –As3–O11 ^{iv}	110.12(10)
O2–As1–O6	110.96(10)	O9 ⁱⁱⁱ –As2–O10 ⁱ	110.37(10)	O4–As3–O11 ^{iv}	113.64(10)
O3–As1–O7	108.45(10)	O1–As2–O12 ⁱⁱ	108.99(10)	O8 ^{vi} –As3–O5 ^v	109.28(10)
O2–As1–O7	109.16(10)	O9 ⁱⁱⁱ –As2–O12 ⁱⁱ	110.58(10)	O4–As3–O5 ^v	107.41(11)
O3–As1–O2	109.25(10)	O9 ⁱⁱⁱ –As2–O1	101.65(9)	O4–As3–O8 ^{vi}	103.87(10)
<O–As1–O>	109.45	<O–As2–O>	109.43	<O–As3–O>	109.41
Zn-Polyhedra					
O1 ^{vii} –Zn1–OW1	93.86(9)	O12–Zn3–O6	94.28(9)	O9–Zn4–O2	103.44(8)
O1–Zn1–OW1	86.14(8)	O11–Zn3–O6	98.21(9)	O7 ^x –Zn4–O2	94.97(8)
O8 ⁱⁱⁱ –Zn1–OW1 ^{vii}	80.24(8)	O5–Zn3–O6	89.80(9)	OW2–Zn4–O2	89.20(9)
O8 ⁱⁱⁱ –Zn1–OW1	99.76(8)	OW1–Zn3–O6	76.98(8)	O10–Zn4–O2	78.49(8)
O1 ^{vii} –Zn1–OW1 ^{vii}	86.14(9)	O1–Zn3–O12	108.66(9)	O9–Zn4–O7 ^{ix}	91.44(8)
O1 ^{vii} –Zn1–OW1	93.86(8)	O11–Zn3–O12	112.01(9)	O7 ^{ix} –Zn4–O7 ^x	84.94(8)
O8 ^{viii} –Zn1–OW1 ^{vii}	99.76(8)	O5–Zn3–O12	73.26(8)	OW2–Zn4–O7 ^{ix}	92.80(9)
O8 ^{viii} –Zn1–OW1	80.24(8)	O11–Zn3–O1	94.68(9)	O10–Zn4–O7 ^x	86.53(8)
O8 ⁱⁱⁱ –Zn1–O1	89.87(8)	O5–Zn3–O1	75.30(8)	O7 ^x –Zn4–O9	82.49(8)
O8 ⁱⁱⁱ –Zn1–O1 ^{vii}	90.13(8)	OW1–Zn3–O1	77.14(8)	OW2–Zn4–O9	89.89(9)
O8 ^{viii} –Zn1–O1	90.13(8)	OW1–Zn3–O11	75.68(8)	O10–Zn4–O7 ^{ix}	86.79(8)
O8 ^{viii} –Zn1–O1 ^{vii}	89.87(8)	OW1–Zn3–O5	100.33(8)	O10–Zn4–OW2	100.77(9)
<O–Zn1–O>	90.00	<O–Zn3–O>	89.69	<O–Zn4–O>	90.15
O8–Zn2–O3	121.48(9)			O4 ^x –Zn5–O5	127.26(9)
O9–Zn2–O3	111.24(9)			O2–Zn5–O5	108.30(10)
O4–Zn2–O3	108.00(9)			O10–Zn5–O5	106.93(9)
O9–Zn2–O8	102.60(8)			O12–Zn5–O5	78.62(8)
O4–Zn2–O8	108.53(8)			O2–Zn5–O4 ^x	121.58(8)
O4–Zn2–O9	103.52(8)			O10–Zn5–O4 ^x	95.35(9)
<O–Zn2–O>	109.23			O12–Zn5–O4 ^x	83.34(8)
				O10–Zn5–O2	83.32(8)
				O12–Zn5–O2	92.07(8)
				<O–Zn5–O>	99.64

symmetry code: (i) -x+1, -y+1, -z+1; (ii) -x, -y+1, -z+1; (iii) x-1, y, z+1; (iv) x+1, y, z-1; (v) x, y, z-1; (vi) -x+1, -y+2, -z-1; (vii) -x, -y+2, -z+1; (viii) -x+1, -y+2, -z; (ix) x+1, y, z; (x) -x+1, -y+1, -z;

Results

Table 19. Bond valences for $Zn_9(AsO_4)_6(H_2O)_4$ calculated after Brese and O’Keeffe, (1991) and for hydrogen atoms after Ferraris and Ivaldi, (1988).

	As1	As2	As3	Zn1 [6]	Zn2 [4]	Zn3 [6]	Zn4 [6]	Zn5 [5]	Σ_{vij}^*
O1	—	1.19	—	0.36×2↓	—	0.41	—	—	1.96
O2	1.19	—	—	—	—	—	0.37	0.45	2.01
O3	1.24	—	—	—	0.6	—	—	—	1.84
O4	—	—	1.20	—	0.48	—	—	0.48	2.16
O5	—	—	1.30	—	—	0.15	—	0.54	1.99
O6	1.29	—	—	—	—	0.47	—	—	1.76
O7	1.24	—	—	—	—	—	0.36+0.32	—	1.92
O8	—	—	1.20	0.24×2↓	0.53	—	—	—	1.97
O9	—	1.13	—	—	0.48	—	0.33	—	1.94
O10	—	1.29	—	—	—	—	0.28	0.39	1.96
O11	—	—	1.34	—	—	0.4	—	—	1.74
O12	—	1.27	—	—	—	0.42	—	0.23	1.92
OW1	—	—	—	0.37×2↓	—	0.12	—	—	0.49
OW2	—	—	—	—	—	—	0.31	—	0.31
Σ_{vij}	4.96	4.88	5.04	1.94	2.09	1.97	1.97	2.09	

	Σ_{vij}^*	H1A	H1B	H2A	H2B	Σ_{vij}^{**}
O1	1.96	—	—	—	—	1.96
O2	2.01	—	—	—	—	2.01
O3	1.84	0.20	—	—	—	2.04
O4	2.16	—	—	—	—	2.16
O5	1.99	—	—	—	—	1.99
O6	1.76	—	—	0.16	—	1.92
O7	1.92	—	—	—	—	1.92
O8	1.97	—	—	—	—	1.97
O9	1.94	—	0.14	—	—	2.08
O10	1.96	—	—	—	—	1.96
O11	1.74	—	—	—	0.16	1.90
O12	1.92	—	—	—	—	1.92
OW1	0.49	0.80	0.86	—	—	2.15
OW2	0.31	—	—	0.84	0.84	1.99
Σ_{vij}		1.00	1.00	1.00	1.00	

* without H input, ** with H input

Results

Table 20. Disorder indices (Baur, 1974) of the Zn-polyhedra and As-tetrahedra for $Zn_9(AsO_4)_6(H_2O)_4$.

As-tetrahedra					
<As1-O>	1.687	<As2-O>	1.695	<As3-O>	1.682
<O-As1-O>	109.45	<O-As2-O>	109.43	<O-As3-O>	109.41
<O-O>	2.75	<O-O>	2.76	<O-O>	2.76
DI(As1-O)	0.0045	DI(As2-O)	0.0107	DI(As3-O)	0.0105
DI(O-As1-O)	0.0143	DI(O-As2-O)	0.0252	DI(O-As3-O)	0.0232
DI(O-O)	0.0100	DI(O-O)	0.0169	DI(O-O)	0.0117
Zn-polyhedra					
<Zn1-O>	2.125	<Zn3-O>	2.160	<Zn5-O>	2.038
<O-Zn1-O>	90.00	<O-Zn3-O>	89.69	<O-Zn5-O>	99.64
<O-O>	3.00	<O-O>	3.03	<O-O>	3.06
DI(Zn1-O)	0.0314	DI(Zn3-O)	0.0848	DI(Zn5-O)	0.0418
DI(O-Zn1-O)	0.0509	DI(O-Zn3-O)	0.1303	DI(O-Zn5-O)	0.1461
DI(O-O)	0.0445	DI(O-O)	0.0790	DI(O-O)	0.0807
<Zn2-O>	1.948	<Zn4-O>	2.116		
<O-Zn2-O>	109.23	<O-Zn4-O>	90.15		
<O-O>	3.17	<O-O>	2.99		
DI(Zn2-O)	0.0153	DI(Zn4-O)	0.0123		
DI(O-Zn2-O)	0.0435	DI(O-Zn4-O)	0.0604		
DI(O-O)	0.0224	DI(O-O)	0.0449		
DI(TO) _{tet} = (Σ TO _i - TO _m)/4TO _m		DI(OTO) _{tet} = (Σ OTO _i - OTO _m)/6OTO _m		DI(OO) _{tet} = (Σ OO _i - OO _m)/6OO _m	
DI(TO) _{oct} = (Σ TO _i - TO _m)/6TO _m		DI(OTO) _{oct} = (Σ OTO _i - OTO _m)/12OTO _m		DI(OO) _{oct} = (Σ OO _i - OO _m)/12OO _m	

Table 21. Disorder Parameter (Fleet, 1976; Robinson et al., 1971) for As-tetrahedra and Zn-polyhedra for $Zn_9(AsO_4)_6(H_2O)_4$.

As-tetrahedra	As1	As2	As3
σ_{tet}^2	4.7297	19.2528	12.0314
λ_{tet}	0.4724	0.4812	0.4658
Zn-octahedra	Zn1	Zn3	Zn4
σ_{oct}^2	40.0633	189.5559	51.8414
λ_{oct}	1.2720	1.3849	1.2503
Zn-tetrahedron	Zn2		
σ_{tet}^2	46.6250		
λ_{tet}	0.8957		
$\sigma_{tet}^2 = \frac{1}{5} \Sigma(\angle_i - 109.47^\circ)^2$ $\lambda_{tet} = \frac{1}{4} \Sigma[(l_i - l_m)/l_m]^2$ $\sigma_{oct}^2 = \frac{1}{11} \Sigma(\angle_i - 90^\circ)^2$ $\lambda_{oct} = \frac{1}{6} \Sigma[(l_i - l_m)/l_m]^2$			

4.3.2 Raman Spectra of $\text{Zn}_9(\text{AsO}_4)_6(\text{H}_2\text{O})_4$

Figure 15 shows the Raman spectrum of $\text{Zn}_9(\text{AsO}_4)_6(\text{H}_2\text{O})_4$. At the high-energy range, between 2800 and 3800 cm^{-1} , two weak bands appeared and are assigned to the stretching vibrations of the O–H bonds of the hydroxyl groups. The bands are centered around 2963 and 3347 cm^{-1} . According to Libowitzky (1999), the lengths of hydrogen bonds correlate with O–H stretching frequencies. The bands agree well with the refined O–H \cdots O bond lengths (Table 17) and indicate intermediately strong to weak hydrogen bonds.

In the lower energy range, between 100-1200 cm^{-1} , the bands are assigned to the internal vibrations of the AsO_4 tetrahedra. The symmetric and antisymmetric stretching modes of the $(\text{AsO}_4)^{3-}$ groups range from 700-1000 cm^{-1} and the bending modes are located in the area below 550 cm^{-1} and are partially overlain by various external vibrational modes. The most intense Raman bands are located at 910, 878, 830 and 794 cm^{-1} . Compared to the Raman spectrum of the mineral Adamite (ruff.info) the most intense stretching modes of the $(\text{AsO}_4)^{3-}$ groups (at 910, 878 and 830 cm^{-1}) of $\text{Zn}_9(\text{AsO}_4)_6(\text{H}_2\text{O})_4$ are located in a higher energy range than the stretching modes of the $(\text{AsO}_4)^{3-}$ groups of the mineral adamite, which are located at 888, 845 and 794 cm^{-1} .

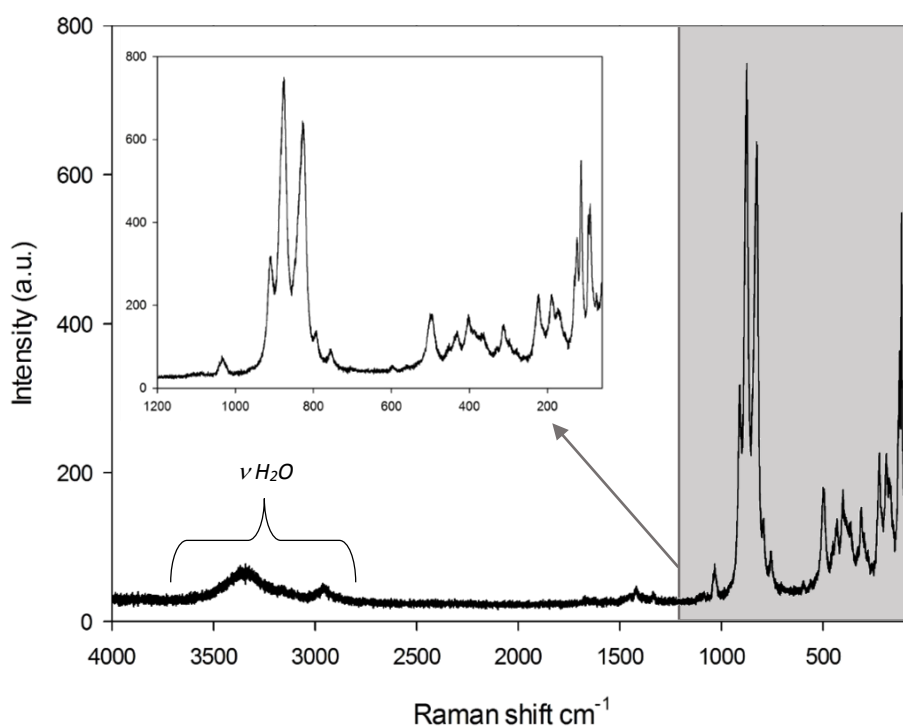


Figure 15. Raman spectrum of $\text{Zn}_9(\text{AsO}_4)_6(\text{H}_2\text{O})_4$.

Results

4.4 $\text{Cd}_{4.65}\text{Ni}_{0.35}(\text{H}_2\text{O})_4(\text{AsO}_4)_2(\text{HAsO}_4)_2$

$\text{Cd}_{4.65}\text{Ni}_{0.35}(\text{H}_2\text{O})_4(\text{AsO}_4)_2(\text{HAsO}_4)_2$ was hydrothermally synthesised at 120°C. The crystals are light green, prismatic with a maximum length of 0.15 mm. EDS analyses confirm the presence of Cd, Ni, As and O with a ratio of (Cd+Ni):As close to 1.25 (Table 5). The concentration of Ni is bigger than the refined value from the XRD data. It varies between different single crystals.

$\text{Cd}_{4.65}\text{Ni}_{0.35}(\text{H}_2\text{O})_4(\text{AsO}_4)_2(\text{HAsO}_4)_2$ adopts a mineral-like structure and is isostructural with the miguelromeroite-sainfeldite series, $\text{Mn}_5(\text{AsO}_4)_2(\text{HAsO}_4)_2 \cdot 4\text{H}_2\text{O}$ – $\text{Ca}_5(\text{AsO}_4)_2(\text{HAsO}_4)_2 \cdot 4\text{H}_2\text{O}$ (Ferraris and Abbona, 1972; Kampf, 2009; Stock et al., 2002). All these minerals have a hureaulite structure type, $\text{Mn}_5(\text{PO}_4)_2(\text{HPO}_4)_2 \cdot 4\text{H}_2\text{O}$ (Menchetti and Sabelli, 1973). The pure pentacadmium dihydrogen tetrakisarsenate tetrahydrate, $\text{Cd}_5(\text{AsO}_4)_2(\text{HAsO}_4)_2 \cdot 4\text{H}_2\text{O}$, which was published by Johnson et al. (2003), has a structure equivalent to the new compound.

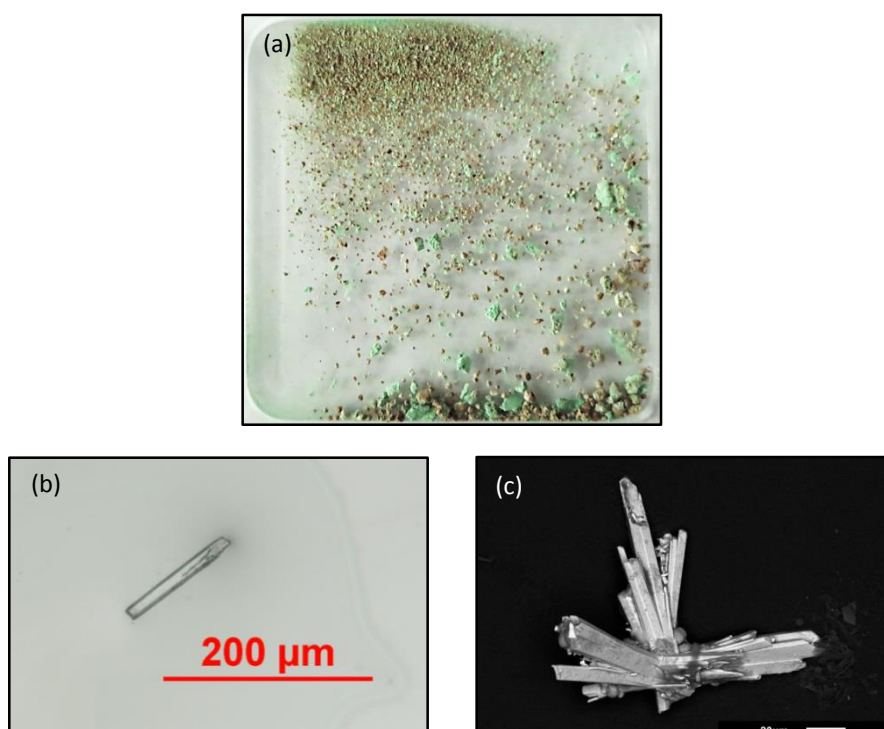


Figure 16. The sample material with $\text{Cd}_{4.65}\text{Ni}_{0.35}(\text{H}_2\text{O})_4(\text{AsO}_4)_2(\text{HAsO}_4)_2$ (a) and the single crystal (b, c). Right Image (b) is taken with a light microscope, left image (c) is a BSE-image of $\text{Cd}_{4.65}\text{Ni}_{0.35}(\text{H}_2\text{O})_4(\text{AsO}_4)_2(\text{HAsO}_4)_2$.

Results

4.4.1 Structure description

The crystal structure of $\text{Cd}_{4.65}\text{Ni}_{0.35}(\text{H}_2\text{O})_4(\text{AsO}_4)_2(\text{HASO}_4)_2$ has three crystallographically distinct divalent cations with octahedral coordination (Cd1, M2 and Cd3). M1 is located at a special position with a half-occupancy which is located on the two-fold axis. M2 and Cd3 have a general position. Cd1 and Cd3 are fully occupied by Cd but M2 is only partially occupied by 83% Cd and 17% Ni.

The Cd–O distances for the Cd1O_6 octahedron are in the range of 2.239(4) Å to 2.333(3) Å (average value of 2.2880 Å) and the Cd3–O distances vary between 2.235(3) Å and 2.399(4) Å (average value of 2.3048 Å). The $\text{Cd}_{0.83}\text{Ni}_{0.17}$ –O distances are slightly shorter because of the substitution of Cd2 by the smaller Ni2. The values range from 2.205(4) Å to 2.375(4) Å (average value of 2.2585 Å).

The three different octahedra are forming an edge-sharing five-membered chain $(\text{Cd}_{2.83}\text{Ni}_{2.17})\text{O}_4(\text{OH}_2)_2\text{--Cd3O}_6\text{--Cd1O}_6\text{--Cd3O}_6\text{--}(\text{Cd}_{2.83}\text{Ni}_{2.17})\text{O}_4(\text{OH}_2)_2$ (Figure 17). The octahedron in the middle, Cd1O_6 , shares all its six oxygen atoms with AsO_4 tetrahedra and two edges with the Cd3O_6 octahedra. Each one of the two Cd3O_6 octahedra shares five of its oxygens atoms with AsO_4 tetrahedra, one edge with Cd1O_6 , another edge with $(\text{Cd}_{2.83}\text{Ni}_{2.17})\text{O}_4(\text{OH}_2)_2$ and two corners (O4, O10) with Cd3O_6 octahedra of adjacent chains. The two $(\text{Cd}_{2.83}\text{Ni}_{2.17})\text{O}_4(\text{OH}_2)_2$ octahedra share four of their oxygen atoms with AsO_4 tetrahedra, one edge with the Cd3O_6 octahedron of the same chain and two edges (O4 and O10) with different Cd3O_6 octahedra of adjacent chains. Two corners of the $(\text{Cd}_{2.83}\text{Ni}_{2.17})\text{O}_4(\text{OH}_2)_2$ and one corner of the Cd3O_6 are occupied by the oxygen atoms O9 and O10 which are the two oxygen atoms of the water molecules in the structure.

As already mentioned the whole structure is linked together *via* two corners (O4, O10) of the octahedra chains. Furthermore, the structure is linked *via* AsO_4 and AsO_3OH tetrahedra between the octahedra chains (Figure 17).

The two distinct As cations form two different tetrahedra, HAS1O_4 and As2O_4 . All corners of the two tetrahedra are connected with the adjacent Cd octahedra. The As–O distances are in the range from 1.669(3) Å to 1.723(3) Å for HAS1O_4 and from 1.673(3) Å to 1.698(3) Å for

Results

As_2O_4 . Only the As1-OH bond with a distance of $1.723(4)$ Å is considerable longer than the other As-O distances due to the OH group. The average $\langle\text{As-O}\rangle$ bond distance and average $\langle\text{O-As-O}\rangle$ bond angle is 1.686 Å and 109.46° for HAsO_4 and 1.687 Å and 109.46° for As_2O_4 . All detailed bonding information is listed in Table 24 and Table 26.

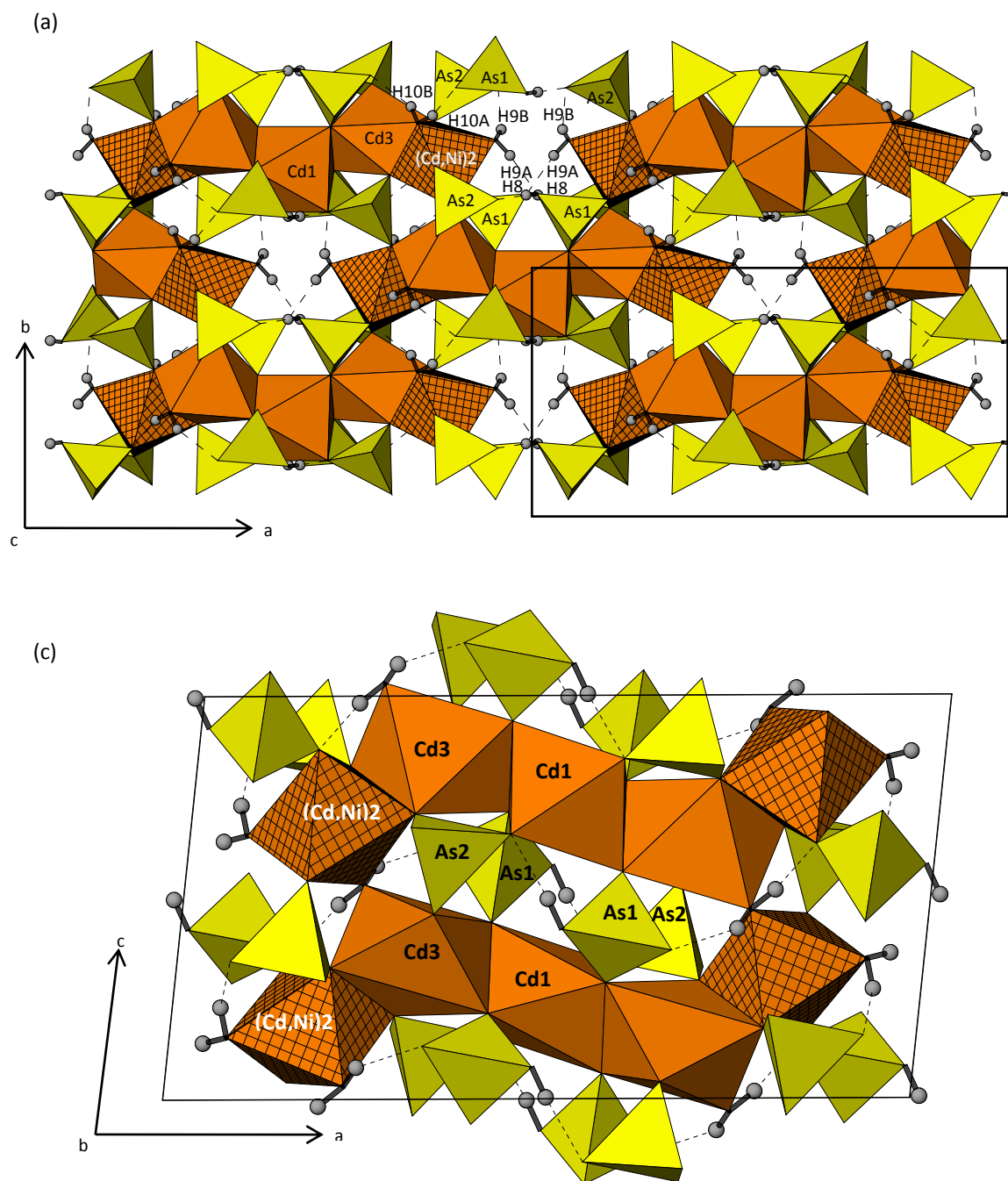


Figure 17. Image of the structure of $\text{Cd}_{4.65}\text{Ni}_{0.35}(\text{H}_2\text{O})_4(\text{AsO}_4)_2(\text{HAsO}_4)_2$ along $[001]$ (a) and along $[010]$ (b). The five octahedra are connected by AsO_4 and HAsO_4 tetrahedra together with hydrogen bonds.

Results

In the structure five different hydrogen bonds are present involving the oxygen atoms O8, O9 and O10 as hydrogen bond donor and O2, O7, and O8 as hydrogen bond acceptor. The hydrogen bond O8–H8···O7 is a short and linear hydrogen bond (with O8···O7 = 2.657(5) Å and O8–H8···O7 = 175°). It is the strongest hydrogen bond in the structure. The other four hydrogen bonds involve the two oxygen atoms O9 and O10 from the two water molecules. O9 and O10 act as double bond donor to either O7 and O8 or to two symmetry equivalents of O2, respectively. Due to the D···A distances in the range of 2.677(5) Å to 2.851(5) Å the bonds are considered as strong to intermediately strong hydrogen bonds. The calculations of the bond valences also confirm the location of the hydrogen bonds. All oxygen atoms which are included in hydrogen bonding are undersaturated (for detailed values Table 25). The values for the other oxygen atoms are close to the nominal valence of 2+.

Table 22. Fractional atomic coordinates of Cd_{4.65}Ni_{0.35}(H₂O)₄(AsO₄)₂(HAsO₄)₂ and displacement parameters. U_{equiv} according to *Fischer and Tillmanns, (1988)*. For the H atoms U_{iso} is shown.

Site	Atom	Wyckoff	x	y	z	U_{eq} / U_{iso}	sof
1							
Cd1	Cd	4e	0.5000	0.39375(6)	0.7500	0.01629(12)	0.5
M2	Cd	8f	0.68169(2)	0.91448(4)	0.81576(4)	0.01609(13)	0.826(5)
M2	Ni	8f	0.68169(2)	0.91448(4)	0.81576(4)	0.01609(13)	0.174(5)
Cd3	Cd	8f	0.67511(2)	0.52953(4)	0.86647(3)	0.01613(9)	1.0
As1	As	8f	0.58357(3)	0.68394(5)	0.58861(5)	0.01376(11)	1.0
As2	As	8f	0.65986(3)	0.23655(5)	0.62600(5)	0.01287(11)	1.0
O1	O	8f	0.5765(2)	0.5685(4)	0.7122(3)	0.0211(8)	1.0
O2	O	8f	0.66051(18)	0.7753(4)	0.6316(3)	0.0209(8)	1.0
O3	O	8f	0.41595(19)	0.3916(4)	0.5627(3)	0.0218(8)	1.0
O4	O	8f	0.66314(19)	0.7409(4)	0.9582(3)	0.0185(7)	1.0
O5	O	8f	0.79456(18)	0.5891(4)	0.8257(3)	0.0174(7)	1.0
O6	O	8f	0.70160(19)	0.3729(4)	0.7071(3)	0.0209(8)	1.0
O7	O	8f	0.57097(17)	0.2243(4)	0.6567(3)	0.0176(7)	1.0
O8	O	8f	0.5106(2)	0.7982(4)	0.5790(4)	0.0241(8)	1.0
O9	O	8f	0.5768(2)	1.0157(4)	0.8456(4)	0.0331(10)	1.0
O10	O	8f	0.76019(19)	0.4180(4)	1.0323(3)	0.0212(8)	1.0
H8	O	8f	0.4876	0.7929	0.5040	0.029	
H9A	H	8f	0.5461	0.9523	0.8600	0.040	
H9B	H	8f	0.5645	1.0567	0.7711	0.040	
H10A	H	8f	0.7912	0.3871	0.9828	0.025	
H10B	H	8f	0.7458	0.3513	1.0790	0.025	

Results

The degree of distortion of the tetrahedra and octahedra was calculated by using the three distortion indices (DI) by Baur (1974) (Equation 1) and furthermore, the disorder parameters bond angle variance (σ^2) and mean quadratic elongation (λ) introduced by Robinson et al. (1971) and Fleet (1976) (Equation 2) were determined (Table 27 and Table 28).

Similar to the zinc arsenate structure, $Zn_9(AsO_4)_6(H_2O)_4$, the octahedra are much more distorted than the tetrahedra. Especially the angles of the Cd3 octahedra are strongly distorted. It has the highest disorder parameter with $\sigma_{oct}^2 = 209.567$. The other two octahedra are only intermediately distorted. Compared to the calculated distortion indices and disorder parameters of the $Cd_2H_2(AsO_4)_4 \cdot 4H_2O$ structure described by Johnson et al. (2003) the M2 position of $Cd_{4.65}Ni_{0.35}(H_2O)_4(AsO_4)_2(HAsO_4)_2$ which is partially occupied by 83% Cd and 17% Ni is slightly less distorted than the M2 of the cadmium arsenate which is fully occupied by Cd. The distortion indices for the structure described by Johnson et al. (2003) value for $DI(TO) = 0.279$ and for $DI(OTO) = 0.0889$ and the disorder parameters value for $\sigma_{oct}^2 = 104.2901$ and for $\lambda_{oct} = 1,5870$. Furthermore the tetrahedra of $Cd_{4.65}Ni_{0.35}(H_2O)_4(AsO_4)_2(HAsO_4)_2$ are not much distorted but the As1 tetrahedra are more distorted than the As2 tetrahedra due to the attached OH group.

Table 23. Anisotropic displacement parameters for $Cd_{4.65}Ni_{0.35}(H_2O)_4(AsO_4)_2(HAsO_4)_2$ defined as $\exp[-2\pi^2 \sum_{i=1}^3 \sum_{j=1}^3 U_{ij} a_i^* a_j^* h_i h_j]$ according to *Fischer and Tillmanns (1988)*.

Site	U_{11}	U_{22}	U_{33}	U_{23}	U_{13}	U_{12}
Cd1	0.0143(2)	0.0190(3)	0.0154(2)	0.000	0.00103(18)	0.000
Cd2	0.0159(2)	0.0161(2)	0.0164(2)	0.00143(15)	0.00225(14)	0.00022(15)
Ni2	0.0159(2)	0.0161(2)	0.0164(2)	0.00143(15)	0.00225(14)	0.00022(15)
Cd3	0.01491(17)	0.01721(19)	0.01627(18)	-0.00203(14)	0.00175(13)	-0.00071(14)
As1	0.0127(2)	0.0164(3)	0.0122(2)	-0.00017(19)	0.00114(17)	0.0009(2)
As2	0.0117(2)	0.0135(3)	0.0132(2)	0.00031(19)	0.00050(17)	-0.00008(19)
O1	0.0210(18)	0.022(2)	0.0196(18)	0.0071(15)	-0.0029(14)	-0.0019(15)
O2	0.0122(16)	0.032(2)	0.0185(18)	-0.0018(15)	0.0013(13)	-0.0069(16)
O3	0.0186(18)	0.030(2)	0.0161(17)	-0.0049(15)	-0.0001(14)	0.0054(16)
O4	0.0242(18)	0.0194(19)	0.0118(16)	-0.0020(14)	0.0017(13)	0.0044(15)
O5	0.0128(16)	0.0180(19)	0.0218(18)	-0.0060(14)	0.0040(13)	-0.0032(14)
O6	0.0168(17)	0.022(2)	0.0246(19)	-0.0116(15)	0.0059(14)	-0.0012(15)
O7	0.0101(15)	0.0221(19)	0.0206(18)	-0.0004(15)	0.0016(13)	0.0014(14)
O8	0.0223(19)	0.029(2)	0.0199(19)	-0.0059(15)	-0.0039(15)	0.0116(16)
O9	0.025(2)	0.037(3)	0.038(2)	0.017(2)	0.0024(17)	-0.0004(19)
O10	0.0238(19)	0.024(2)	0.0165(18)	0.0013(14)	0.0077(14)	0.0034(16)

Results

Table 24. Selected bond distances (Å) for $\text{Cd}_{4.65}\text{Ni}_{0.35}(\text{H}_2\text{O})_4(\text{AsO}_4)_2(\text{HAsO}_4)_2$.

As-Tetrahedra					
As1–O1	1.669(3)	As2–O6	1.673(3)		
As1–O3 ⁱ	1.673(3)	As2–O5 ⁱⁱⁱ	1.681(3)		
As1–O2	1.677(3)	As2–O4 ^v	1.695(3)		
As1–O8	1.723(3)	As2–O7	1.698(3)		
<As1–O>	1.6855	<As2–O>	1.6868		
Cd/M-Octahedra					
Cd1–O1	2.239(4)	M2–O9	2.205(4)	Cd3–O4	2.235(3)
Cd1–O1 ⁱⁱ	2.239(4)	M2–O6 ^{vi}	2.217(3)	Cd3–O6	2.273(3)
Cd1–O3	2.292(3)	M2–O4	2.232(3)	Cd3–O1	2.278(4)
Cd1–O3 ⁱⁱ	2.292(3)	M2–O5 ^{vi}	2.256(3)	Cd3–O3 ⁱⁱ	2.299(4)
Cd1–O7	2.333(3)	M2–O2	2.266(4)	Cd3–O5	2.345(3)
Cd1–O7 ⁱⁱ	2.333(3)	M2–O10 ^{iv}	2.375(4)	Cd3–O10	2.399(4)
<Cd1–O>	2.2880	<M2–O>	2.2585	<Cd3–O>	2.3048

Symmetry codes: (i) $-x+1, -y+1, -z+1$; (ii) $-x+1, y, -z+3/2$; (iii) $-x+3/2, y-1/2, -z+3/2$; (iv) $x-1/2, y-1/2, z$; (v) $-x+1, y-1, -z+3/2$; (vi) $-x+3/2, -y+3/2, -z+2$;

Hydrogen bonds				
D–H⋯A	D–H (Å)	H⋯A (Å)	D⋯A (Å)	D–H⋯A (°)
O8–H8⋯O7	0.82	1.84	2.657(5)	175.0
O9–H9B⋯O7	0.85	1.98	2.735(5)	148.5
O9–H9A⋯O8	0.85	1.94	2.776(5)	169.2
O10–H10B⋯O2	0.85	2.09	2.851(5)	149.2
O10–H10A⋯O2	0.85	1.86	2.677(5)	162.8

Table 25. Bond valences of $\text{Cd}_{4.65}\text{Ni}_{0.35}(\text{H}_2\text{O})_4(\text{AsO}_4)_2(\text{HAsO}_4)_2$ calculated after Brese and O’Keeffe, (1991) and for hydrogen atoms after Ferraris and Ivaldi, (1988).

	As1	As2	Cd1 [6]	M2 [6]	Cd3 [6]	Σ_{vij}^*	H8	H9A	H9B	H10A	H10B	Σ_{vij}^{**}
O1	1.30	—	0.402↓	—	0.36	2.10	—	—	—	—	—	2.10
O2	1.28	—	—	0.38	—	1.66	—	—	—	0.13	0.18	1.97
O3	1.29	—	0.35×2↓	—	0.34	2.33	—	—	—	—	—	2.33
O4	—	1.21	—	0.41	0.41	2.03	—	—	—	—	—	2.03
O5	—	1.26	—	0.39	0.30	1.95	—	—	—	—	—	1.95
O6	—	1.29	—	0.43	0.37	2.09	—	—	—	—	—	2.09
O7	—	1.21	0.31×2↓	—	—	1.83	0.19	—	0.15	—	—	2.17
O8	1.13	—	—	—	—	1.13	0.81	0.17	—	—	—	1.30
O9	—	—	—	0.44	—	0.44	—	0.83	0.85	—	—	2.12
O10	—	—	—	0.28	0.26	0.54	—	—	—	0.87	0.82	2.23
Σ_{vij}	5	4.97	2.12	2.33	1.97		1.00	1.00	1.00	1.00	1.00	

* without H input, ** with H input

Results

Table 26. Selected bond angles (°) for Cd_{4.65}Ni_{0.35}(H₂O)₄(AsO₄)₂(HAsO₄)₂.

As-Tetrahedra					
O3 ⁱ -As1-O1	113.00 (18)	O5 ⁱⁱⁱ -As2-O6	108.90 (18)		
O2-As1-O1	106.53 (17)	O4 ^v -As2-O6	108.39 (17)		
O8-As1-O1	109.69 (18)	O7-As2-O6	111.46 (17)		
O2-As1-O3 ⁱ	111.60 (18)	O4 ^v -As2-O5 ⁱⁱⁱ	108.62 (17)		
O8-As1-O3 ⁱ	107.57 (17)	O7-As2-O5 ⁱⁱⁱ	110.50 (17)		
O8-As1-O2	108.37 (19)	O7-As2-O4 ^v	108.91 (17)		
<O-As1-O>	109.46	<O-As2-O>	109.46		
Cd/M-Octahedra					
O1 ⁱⁱ -Cd1-O1	83.76 (19)	O4-M2-O9	92.46 (14)	O1-Cd3-O4	91.34 (13)
O3-Cd1-O1	104.45 (13)	O5 ^{vi} -M2-O9	89.55 (13)	O3 ⁱⁱ -Cd3-O4	106.47 (13)
O3 ⁱⁱ -Cd1-O1	76.35 (13)	O2-M2-O9	106.84 (14)	O5-Cd3-O4	89.30 (12)
O7-Cd1-O1	93.45 (13)	O10 ^{iv} -M2-O9	87.64 (14)	O10-Cd3-O4	101.72 (12)
O3-Cd1-O1 ⁱⁱ	76.35 (13)	O4-M2-O6 ^{vi}	98.55 (13)	O1-Cd3-O6	81.33 (13)
O3 ⁱⁱ -Cd1-O1 ⁱⁱ	104.45 (13)	O5 ^{vi} -M2-O6 ^{vi}	79.24 (12)	O3 ⁱⁱ -Cd3-O6	93.25 (13)
O7 ⁱⁱ -Cd1-O1 ⁱⁱ	93.45 (13)	O2-M2-O6 ^{vi}	83.98 (13)	O5-Cd3-O6	76.28 (12)
O7 ⁱⁱ -Cd1-O3 ⁱⁱ	91.42 (12)	O10 ^{iv} -M2-O6 ^{vi}	79.21 (13)	O10-Cd3-O6	91.04 (12)
O7 ⁱⁱ -Cd1-O3	87.86 (12)	O2-M2-O4	93.27 (13)	O3 ⁱⁱ -Cd3-O1	75.46 (12)
O7-Cd1-O3 ⁱⁱ	87.86 (12)	O10 ^{iv} -M2-O4	100.47 (12)	O5-Cd3-O1	122.32 (13)
O7-Cd1-O3	91.42 (12)	O2-M2-O5 ^{vi}	87.31 (13)	O10-Cd3-O3 ⁱⁱ	88.62 (12)
O7 ⁱⁱ -Cd1-O7	92.30(17)	O10 ^{iv} -M2-O5 ^{vi}	78.39 (13)	O10-Cd3-O5	70.99 (12)
<O-Cd1-O>	90.26	<O-M2-O>	89.74	<O-Cd3-O>	90.68

Symmetry codes: (i) -x+1, -y+1, -z+1; (ii) -x+1, y, -z+3/2; (iii) -x+3/2, y-1/2, -z+3/2; (iv) x-1/2, y-1/2, z; (v) -x+1, y-1, -z+3/2; (vi) -x+3/2, -y+3/2, -z+2;

Table 27. Disorder indices (Baur, 1974) for Cd_{4.65}Ni_{0.35}(H₂O)₄(AsO₄)₂(HAsO₄)₂ of the M-octahedra and As-tetrahedra.

Cd/M-Octahedra					
<Cd1-O>	2.2880	<M2-O>	2.2585	<Cd3-O>	2.3048
<O-Cd1-O>	90.26	<O-M2-O>	89.74	<O-Cd3-O>	90.68
<O-O>	3.23	<O-O>	3.18	<O-O>	3.25
DI(Cd1-O)	0.0143	DI(M2-O)	0.0183	DI(Cd3-O)	0.0194
DI(O-Cd1-O)	0.0722	DI(O-M2-O)	0.0796	DI(O-Cd3-O)	0.1141
DI(O-O)	0.0600	DI(O-O)	0.0573	DI(O-O)	0.0870
As-Tetrahedra					
<As1-O>	1.6855	<As2-O>	1.6868		
<O-As1-O>	109.46	<O-As2-O>	109.46		
<O-O>	2.75	<O-O>	2.75		
DI(As1-O)	0.0111	DI(As2-O)	0.0058		
DI(O-As1-O)	0.0180	DI(O-As2-O)	0.0092		
DI(O-O)	0.0100	DI(O-O)	0.0073		
DI(TO) _{tet} = (Σ TO _i - TO _m)/4TO _m		DI(OT) _{tet} = (Σ OTO _i - OTO _m)/6OTO _m		DI(OO) _{tet} = (Σ OO _i - OO _m)/6OO _m	
DI(TO) _{oct} = (Σ TO _i - TO _m)/6TO _m		DI(OT) _{oct} = (Σ OTO _i - OTO _m)/12OTO _m		DI(OO) _{oct} = (Σ OO _i - OO _m)/12OO _m	

Results

Table 28. Disorder parameter (Fleet, 1976; Robinson et al., 1971) for the As-tetrahedra and Zn-polyhedra of $\text{Cd}_{4.65}\text{Ni}_{0.35}(\text{H}_2\text{O})_4(\text{AsO}_4)_2(\text{HAsO}_4)_2$.

As-Tetrahedra	As1	As2	
σ_{tet}^2	6.1020	1.5017	
λ_{tet}	0.4704	0.4717	
Cd/M-Octahedra	Cd1	M2	Cd3
σ_{oct}^2	79.2250	81.7499	209.5668
λ_{oct}	1.6604	1.5870	1.7054

$$\sigma_{tet}^2 = \frac{1}{5} \Sigma(\angle_i - 109.47^\circ)^2 \quad \lambda_{tet} = \frac{1}{4} \Sigma[(l_i - l_m)/l_m]^2 \quad \sigma_{oct}^2 = \frac{1}{11} \Sigma(\angle_i - 90^\circ)^2 \quad \lambda_{oct} = \frac{1}{6} \Sigma[(l_i - l_m)/l_m]^2$$

4.4.2 Raman spectra of $\text{Cd}_{4.65}\text{Ni}_{0.35}(\text{H}_2\text{O})_4(\text{AsO}_4)_2(\text{HAsO}_4)_2$

Figure 18 shows the Raman spectrum of $\text{Cd}_{4.65}\text{Ni}_{0.35}(\text{H}_2\text{O})_4(\text{AsO}_4)_2(\text{HAsO}_4)_2$. The broad band in the high-energy range, between $2100\text{--}3750\text{ cm}^{-1}$, is assigned to the stretching of the O–H bonds of the hydroxyl groups. Based on the $d(\text{H}\cdots\text{O})\text{--}\nu$ correlation described by Libowitzky (1999), the O–H stretching region agrees well with the refined O–H \cdots O bond lengths (Table 24).

The bands which are located in the lower energy range ($100\text{--}1200\text{ cm}^{-1}$) are assigned to the internal vibrations of the AsO_4 tetrahedra. The symmetric and antisymmetric stretching modes of the $(\text{AsO}_4)^{3-}$ groups range from $700\text{--}1000\text{ cm}^{-1}$ and are located at $889, 861, 814$ and 763 cm^{-1} which are the most intense Raman bands. The bending modes are located in the area below 550 cm^{-1} and are partially overlain by various external vibrational modes. Compared to the Raman spectrum of the mineral miguelromeroite (Kampf, 2009) the two stretching modes at 814 cm^{-1} and 763 cm^{-1} of $\text{Cd}_{4.65}\text{Ni}_{0.35}(\text{H}_2\text{O})_4(\text{AsO}_4)_2(\text{HAsO}_4)_2$ are in the lower energy range than the two stretching modes at 833 cm^{-1} and 798 cm^{-1} of the mineral phase (rruff.info).

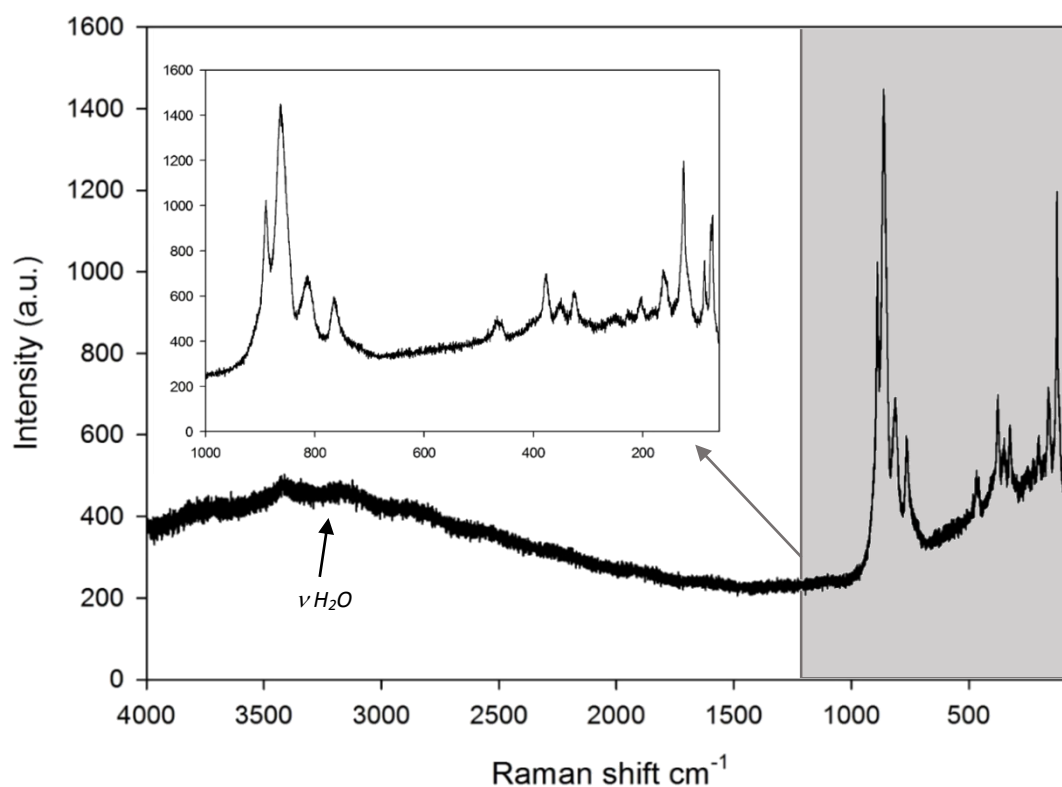


Figure 18. Raman spectrum of $\text{Cd}_{4.65}\text{Ni}_{0.35}(\text{H}_2\text{O})_4(\text{AsO}_4)_2(\text{HAsO}_4)_2$.

5 CONCLUSION

In this Master's thesis the effectiveness of the ionothermal synthesis to produce arsenates which are appropriate for single-crystal structure analysis was tested. Overall 30 syntheses in the system $\text{CdO-MO-As}_2\text{O}_5\text{-(H}_2\text{O/IL)}$ were carried out under four heat treatment gradients (max. temp. 120°C, 140°, 160°C and 220°C), 15 with [emim]Br as solvent and 15 with H₂O as solvent. Finally, 22 crystals with single crystal X-ray diffraction quality were grown, 8 of them with H₂O as the solvent and 14 of them with [emim]Br as the solvent (Table 2).

Using the ionic liquid, [emim]Br as a template an imidazolium bromocadmiate, $(\text{C}_6\text{H}_{11}\text{N}_2)_2[\text{CdBr}_4]$, crystallised in two polymorphic modifications (α - $(\text{C}_6\text{H}_{11}\text{N}_2)_2[\text{CdBr}_4]$ and β - $(\text{C}_6\text{H}_{11}\text{N}_2)_2[\text{CdBr}_4]$). Together with the α - $(\text{C}_6\text{H}_{11}\text{N}_2)_2[\text{CdBr}_4]$ crystallised the zinc arsenate, $\text{Zn}_9(\text{AsO}_4)_3 \cdot 4\text{H}_2\text{O}$. This arsenate was synthesised for the first time using the ionothermal method.

The low-temperature hydrothermal method ($T_{\text{max}}=120^\circ\text{C}$) shows the formation of homogenous single crystals which are appropriate for single-crystal structure analysis by using suitable conditions like a moderate pH value (pH=3-6) and a large amount of water (filling volume 70-90%). A new Cd and Ni bearing arsenate, $\text{Cd}_{4.65}\text{Ni}_{0.35}(\text{H}_2\text{O})_4(\text{AsO}_4)_2(\text{HAsO}_4)_2$, evolved under hydrothermal conditions. It adopts a mineral-like structure with a hureaulite structure type.

The two described synthesis methods were successful in the synthesis of metal bearing arsenates. Besides already known chemical phases, the hydrothermal synthesis also yielded a new mineral related compound and the successful ionothermal synthesis with ionic liquids as solvent and template demonstrates that the method can be used to synthesise more new mineral related arsenates. It also demonstrates that the ionothermal synthesis is a promising method for the synthesis of other environmentally relevant compounds.

Introduction of non-custom synthesis methods in the mineral synthesis like the ionothermal one verify that the synthesis of metal-arsenates is not fully developed yet. Further investigations of their stability under different conditions would be advantageous. Knowing

Conclusion

special crystal structure features of new synthetic phases and their stability under laboratory conditions can be useful for the understanding of the phase behavior under environmental conditions, especially when newly synthesised materials can be compared to natural phases which occur in contaminated soils or drainage ponds. Knowledge of the stability of such phases would bring us one step closer to applications like the successful restoration of mine drainages and contaminated soils.

6 REFERENCES

- Adamite - RRUFF Database: Raman, X-ray, infrared and chemistry [WWW Document]. URL <http://rruff.info/adamite/display=default/R060593> (accessed 06.06.16)
- Anthony, J.L., Brennecke, J.F., Holbrey, J.D., Maginn, E.J., Mantz, R.A., Rogers, R.D., Trulove, P.C., Visser, A.E., Welton, T. (2003). Physicochemical properties of ionic liquids. In: Wasserscheid, P., Welton, T. (Eds.), *Ionic Liquids in Synthesis*. Wiley-VCH Verlag GmbH & Co. KGaA, Weinheim, FRG, pp. 41–126.
- Arsenic: The mineralogy of arsenic [WWW Document], URL <http://www.mindat.org/element/Arsenic> (accessed 11.05.16).
- Barbalace, K. (1995-2016) Periodic table of elements: arsenic - As (EnvironmentalChemistry.com) [WWW Document]. URL <http://environmentalchemistry.com/yogi/periodic/As.html> (accessed 4.21.16a).
- Barbalace, K. (1995-2016) Periodic table of elements: cadmium - Cd (EnvironmentalChemistry.com) [WWW Document]. URL <http://environmentalchemistry.com/yogi/periodic/Cd.html> (accessed 4.21.16b).
- Baur, W.H. (1974). The geometry of polyhedral distortions. Predictive relationships for the phosphate group. *Acta Crystallogr. B* **30**, 5, 1195–1215.
- Beran, A., Voll, D., Schneider, H. (2004). IR spectroscopy as a tool for the characterisation of ceramic precursor phases. In: Beran, A., Libowitzky, E. (Eds.), *Spectroscopic Methods in Mineralogy EMU Notes in Mineralogy*, 6. Eötvös University Press, Budapest, pp. 189–226.
- Bothe, J. V, Brown, P.W. (1999). The stabilities of calcium arsenates at $23\pm 1^\circ\text{C}$. *J. Hazard. Mater.* **69**, 2, 197–207.
- Brese, N.E., O’Keeffe, M. (1991). Bond-valence parameters for solids. *Acta Crystallogr. B* **47**, 2, 192–197.
- Bruker (2007). SAINT+. SAINT+ Bruker AXS Inc., Madison, Wisconsin, USA.
- Byrappa, K., Yoshimura, M. (2013a). Hydrothermal technology—principles and applications. In: *Handbook of Hydrothermal Technology*. Elsevier, pp. 1–49.
- Byrappa, K., Yoshimura, M. (2013b). Apparatus. In: *Handbook of Hydrothermal Technology*. Elsevier, pp. 75–137.
- Cao, S.-W., Zhu, Y.-J., Cui, J.-B. (2010). Iron hydroxyl phosphate microspheres: Microwave-solvothermal ionic liquid synthesis, morphology control, and photoluminescent properties. *J. Solid State Chem.* **183**, 7, 1704–1709.

References

- Chambreau, S.D., Boatz, J. a., Vaghjiani, G.L., Koh, C., Kostko, O., Golan, A., Leone, S.R. (2012). Thermal decomposition mechanism of 1-ethyl-3-methylimidazolium bromide ionic liquid. *J. Phys. Chem. A* **116**, 24, 5867–5876.
- Cullen, W.R., Reimer, K.J. (1989). Arsenic speciation in the environment. *Chem. Rev.* **89**, 4, 713–764.
- Dowty, E. (2006). ATOMS v6.3.1. A complete program for displaying atomic structures. Shape Software, Kingsport, Tennessee, USA.
- Farrugia, L.J. (2012). WinGX and ORTEP for Windows : an update. *J. Appl. Crystallogr.* **45**, 4, 849–854.
- Feng, P., Bu, X., Stucky, G.D. (1997). A synthetic hydrated zinc arsenate constructed from tetrahedral, trigonal bipyramidal and octahedral zinc polyhedra: $[\text{Zn}_3(\text{AsO}_4)_2]_3 \cdot 4\text{H}_2\text{O}$. *Acta Crystallogr. C* **53**, 8, 997–1000.
- Ferraris, G., Abbona, F. (1972). The crystal structure of $\text{Ca}_5(\text{HAsO}_4)_2(\text{AsO}_4)_2 \cdot 4\text{H}_2\text{O}$ (sainfeldite). *Bull. la Société française Minéralogie Cristallogr.* **95**, 33–41.
- Ferraris, G., Ivaldi, G. (1988). Bond valence vs bond length in O–O hydrogen bonds. *Acta Crystallogr. B* **44**, 4, 341–344.
- Fischer, R.X., Tillmanns, E. (1988). The equivalent isotropic displacement factor. *Acta Crystallogr. C* **44**, 4, 775–776.
- Fleet, M.E. (1976). Distortion parameters for coordination polyhedra. *Mineral. Mag.* **40**, 313, 531–533.
- Fry, S.E., Pienta, N.J. (1985). Effects of molten salts on reactions. Nucleophilic aromatic substitution by halide ions in molten dodecyltributylphosphonium salts. *J. Am. Chem. Soc.* **107**, 22, 6399–6400.
- Goldstein, J.I., Newbury, D.E., Echlin, P., Joy, D.C., Lyman, C.E., Lifshin, E., Sawyer, L., Michael, J.R. (2003). Scanning electron microscopy and X-ray microanalysis. Springer US, Boston, MA.
- Gräfe, M., Nachttegaal, M., Sparks, D.L. (2004). Formation of metal-arsenate precipitates at the goethite-water interface. *Environ. Sci. Technol.* **38**, 24, 6561–6570.
- Günzler, H., Heise, H.M. (1996). IR-Spektroskopie: Eine Einführung, 3. ed. VCH Verl.-Ges., Weinheim, Germany.
- Hasan, M., Kozhevnikov, I. V, Siddiqui, M.R.H., Steiner, A., Winterton, N. (1999). Gold compounds as ionic liquids. Synthesis, structures, and thermal properties of N,N' - dialkylimidazolium tetrachloroaurate salts. *Inorg. Chem.* **38**, 25, 5637–5641.
- Hitchcock, P.B., Seddon, K.R., Welton, T. (1993). Hydrogen-bond acceptor abilities of tetrachlorometalate(II) complexes in ionic liquids. *J. Chem. Soc. Dalton Trans.* **17**, 2639.

References

- Järup, L. (2003). Hazards of heavy metal contamination. *Br. Med. Bull.* **68**, 167–182.
- Jensen, T.R., Norby, P., Hanson, J.C., Skou, E.M., Stein, P.C. (1998). Hydrothermal synthesis, crystal structure and thermal transformation of a new zinc arsenate hydrate, $Zn_9(AsO_4)_6 \cdot 4H_2O$. *J. Chem. Soc. Dalton Trans.* **9**, 4, 527–532.
- Jiang, W., Lv, J., Luo, L., Yang, K., Lin, Y., Hu, F., Zhang, J., Zhang, S. (2013). Arsenate and cadmium co-adsorption and co-precipitation on goethite. *J. Hazard. Mater.* **262**, 55–63.
- Johnson, C.D., Skakle, J.M.S., Johnston, M.G., Feldmann, J., Macphee, D.E. (2003). Hydrothermal synthesis, crystal structure and aqueous stability of two cadmium arsenate phases, $CdNH_4(HAsO_4)OH$ and $Cd_5H_2(AsO_4)_4 \cdot 4H_2O$. *J. Mater. Chem.* **13**, 6, 1429.
- Kampf, A.R. (2009). Miguelromeroite, the Mn analogue of sainfeldite, and redefinition of villyaellenite as an ordered intermediate in the sainfeldite-miguelromeroite series. *Am. Mineral.* **94**, 11-12, 1535–1540.
- Katsyuba, S. a., Dyson, P.J., Vandyukova, E.E., Chernova, A. V., Vidiš, A. (2004). Molecular structure, vibrational spectra, and hydrogen bonding of the ionic liquid 1-ethyl-3-methyl-1H-imidazolium tetrafluoroborate. *Helv. Chim. Acta* **87**, 10, 2556–2565.
- Kleber, W., Bautsch, H.-J., Bohm, J., Klimm, D. (2010). Einführung in die Kristallographie. Oldenbourg Verlag.
- Larsen, A.S., Holbrey, J.D., Tham, F.S., Reed, C.A. (2000). Designing ionic liquids: Imidazolium melts with inert carborane anions. *J. Am. Chem. Soc.* **122**, 30, 7264–7272.
- Li, N., Chai, Y., Li, Y., Tang, Z., Dong, B., Liu, Y., Liu, C. (2012). Ionic liquid assisted hydrothermal synthesis of hollow vesicle-like MoS_2 microspheres. *Mater. Lett.* **66**, 1, 236–238.
- Liao, J.-H., Wu, P.-C., Huang, W.-C. (2006). Ionic liquid as solvent for the synthesis and crystallization of a coordination polymer: $(EMI)[Cd(BTC)]$ (EMI = 1-ethyl-3-methylimidazolium, BTC = 1,3,5-benzenetricarboxylate). *Cryst. Growth Des.* **6**, 5, 1062–1063.
- Libowitzky, E. (1999). Correlation of O–H stretching frequencies and O–H...O hydrogen bond lengths in minerals. In: Schuster, P., Mikenda, W. (Eds.), *Hydrogen Bond Research*. Springer Vienna, Vienna, pp. 103–115.
- Libowitzky, E., Beran, A. (2004). IR spectroscopic characterisation of hydrous species in minerals. In: Beran, A., Libowitzky, E. (Eds.), *Spectroscopic Methods in Mineralogy EMU Notes in Mineralogy*, 6. Eötvös University Press, Budapest, pp. 227–279.
- Lin, Z., Wragg, D.S., Morris, R.E. (2006). Microwave-assisted synthesis of anionic metal-organic frameworks under ionothermal conditions. *Chem. Commun. (Camb)*. **4**, 19, 2021–2023.

References

- Liu, L., Yang, J., Li, J., Dong, J., Siřak, D., Luzzatto, M., McCusker, L.B. (2011). Ionothermal synthesis and structure analysis of an open-framework zirconium phosphate with a high CO₂/CH₄ adsorption ratio. *Angew. Chem. Int. Ed. Engl.* **50**, 35, 8139–42.
- Martínez-Palou, R. (2010). Microwave-assisted synthesis using ionic liquids. *Mol. Divers.* **14**, 1, 3–25.
- Massa, W. (2004). Crystal structure determination. Springer-Verlag, Berlin Heidelberg New York.
- Massa, W. (2011). Kristallstrukturbestimmung. Vieweg+Teubner, Wiesbaden.
- Menchetti, S., Sabelli, C. (1973). The crystal structure of hureaulite, Mn₅(HOPO₃)₂(PO₄)₂(H₂O)₄. *Acta Crystallogr. B* **29**, 11, 2541–2548.
- Miguelromeroite - RRUFF Database: Raman, X-ray, infrared and chemistry [WWW Document]. URL <http://rruff.info/miguelromeroite/display=default/> (accessed 12.05.16)
- Moosavi, F. (2013). Ionic liquids - New aspects for the future. InTech.
- Morris, R.E. (2009). Ionothermal synthesis--ionic liquids as functional solvents in the preparation of crystalline materials. *Chem. Commun. (Camb)*. 21, 2990–2998.
- Muntau, H., Baudo, R. (1992). Sources of cadmium, its distribution and turnover in the freshwater environment. *IARC Sci. Publ.* 118, 133–148.
- Nasdala, L., Smith, D.C., Kaindl, R., Ziemann, M.A. (2004). Raman spectroscopy: Analytical perspectives in mineralogical research. In: Beran, A., Libowitzky, E. (Eds.), *Spectroscopic Methods in Mineralogy EMU Notes in Mineralogy*, 6. Eötvös University Press, Budapest, pp. 281–343.
- Nonius (1999). COLLECT data collection software. Nonius BV, Delft, the Netherlands.
- Nordstrom, D.K. (2011). Mine waters: Acidic to circumneutral. *Elements* **7**, 6, 393–398.
- O'Day, P.A. (2006). Chemistry and mineralogy of arsenic. *Elements* **2**, 2, 77–83.
- Otwinowski, Z., Borek, D., Majewski, W., Minor, W. (2003). Multiparametric scaling of diffraction intensities. *Acta Crystallogr. Sect. A Found. Crystallogr.* **59**, 3, 228–234.
- Parnham, E.R., Slawin, A.M.Z., Morris, R.E. (2007). Ionothermal synthesis of β-NH₄AlF₄ and the determination by single crystal X-ray diffraction of its room temperature and low temperature phases. *J. Solid State Chem.* **180**, 1, 49–53.
- Raman, C. V., Krishnan, K.S. (1928). A new type of secondary radiation. *Nature* **121**, 3048, 501–502.
- Reeder, R.J., Schoonen, M. A. A., Lanzirotti, A. (2006). Metal speciation and its role in bioaccessibility and bioavailability. *Rev. Mineral. Geochemistry* **64**, 1, 59–113.

References

- Robinson, K., Gibbs, G. V, Ribbe, P.H. (1971). Quadratic elongation: A quantitative measure of distortion in coordination polyhedra. *Science (80-)*. **172**, 3983, 567–570.
- Rogalski, M., Modarelli, A., Magri, P., Mutelet, F., Grydziusko, A., Wlazło, M., Domańska, U. (2013). Physico-chemical properties and phase behavior of the ionic liquid- β -cyclodextrin complexes. *Int. J. Mol. Sci.* **14**, 8, 16638–16655.
- Sharma, R.P., Sharma, R., Bala, R., Salas, J.M., Quiros, M. (2006). Second sphere coordination complexes via hydrogen bonding: Synthesis, spectroscopic characterisation of [trans-Co(en)₂Cl₂]CdX₄ (X=Br or I) and single crystal X-ray structure determination of [trans-Co(en)₂Cl₂]CdBr₄. *J. Mol. Struct.* **794**, 1-3, 341–347.
- Sheldrick, G.M. (2008). A short history of SHELX. *Acta Crystallogr. A* **64**, 1, 112–122.
- Stock, N., Stucky, G.D., Cheetham, A.K. (2002). Synthesis and characterization of the synthetic minerals Villyaellenite and Sarkinite, Mn₅(AsO₄)₂(HAsO₄)₂·4H₂O and Mn₂(AsO₄)(OH). *Z. Anorg. Allg. Chem.* **5**, 628, 357–362.
- Strunz, H., Nickel, E. (2001). Strunz mineralogical tables. Chemical-structural mineral classification system, 9th ed. Schweizerbart'sche Verlagsbuchhandlung, Stuttgart, Germany.
- Tait, S., Osteryoung, R. a (1984). Infrared study of ambient-temperature chloroaluminates as a function of melt acidity. *Inorg. Chem.* **23**, 25, 4352–4360.
- Taylor, P., Jalali, M., Khanlari, Z. V (2008). Cadmium availability in calcareous soils of agricultural lands in Hamadan, Western Iran. *Soil Sediment Contam.* **17**, 3, 256–268.
- Tian, G. (2012). Application of ionic liquids in extraction and separation of metals. In: Mohammad, A., Inamuddin, D. (Eds.), Green Solvents II. Springer Netherlands, Dordrecht, pp. 119–153.
- Wasserscheid P., Keim W. (2000). Ionic liquids-New “solutions” for transition metal catalysis. *Angew. Chem. Int. Ed. Engl.* **39**, 21, 3772–3789.
- Wragg, D.S., Slawin, A.M.Z., Morris, R.E. (2009). The role of added water in the ionothermal synthesis of microporous aluminium phosphates. *Solid State Sci.* **11**, 2, 411–416.
- Xu, Y.-P., Tian, Z.-J., Wang, S.-J., Hu, Y., Wang, L., Wang, B.-C., Ma, Y.-C., Hou, L., Yu, J.-Y., Lin, L.-W. (2006). Microwave-enhanced ionothermal synthesis of aluminophosphate molecular sieves. *Angew. Chemie* **118**, 24, 4069–4074.

7 ACKNOWLEDGMENT

First of all I want thank Tamara Đorđević for the possibility to participate in her project, for suggesting the topic of the thesis, for giving me the chance to get an insight into the scientific world and for the support over the entire period. She was always there to give me the appropriate answers to my questions, whether they were of a professional nature or aspects of daily life.

I also want thank Ronald Miletich-Pawliczek for the official supervision of my thesis. Furthermore I would like to thank all who helped me with my measurements and the interpretation of my results: Gerald Giester for the single crystal diffraction measurements, Eugen Libowitzky for the infrared light measurements, Andreas Artač for the Raman measurements and Herta Effenberger for answering several questions regarding the computer programs ShelX and Atoms.

A big thank you goes to Florian Steindl for the support over the whole time, for the patience and for proofreading. Also a big thank you goes to my family and friends for their support.

The financial support of the Austrian Science Foundation (FWF) (Grant V203-N19) is gratefully acknowledged.

8 INDEPENDENCE DECLARATION

I hereby declare on oath that I composed this thesis completely on my own and without improper aid by third persons. All references are appropriately cited.

Ich erkläre hiermit an Eides statt, dass ich die vorliegende Thesis selbständig und ohne unzulässige fremde Hilfe angefertigt habe. Die verwendeten Quellen sind vollständig zitiert.